



**POLITECNICO  
DI TORINO**

# Surface Wave Analysis using an innovative acquisition scheme

**Master of Science in Petroleum Engineering**  
Domenico Maria Crisafulli

Supervisor: Prof. Laura Valentina Socco  
Co-Supervisor: Farbod Khosro Anjom

Politecnico Di Torino  
Department of Environment, Land and Infrastructure Engineering

**March 2021**

## **ACKNOWLEDGEMENTS**

I would like to thank Total E&P to provide the dataset.

I would like to thank my supervisor, Laura Valentina Socco whose expertise was invaluable in formulating the research questions and methodology.

I would like to acknowledge Khosro Anjom Farbod for his guidance and patience through each stage of the process.

I would like to thank my mother and my sister for their wise counsel and support.

In addition, I would like to thank Fabio, Francesco and Luna.

## ABSTRACT

We present a seismic three-dimensional case study, from the mining site in the province of Aurignac, south France, characterized by stiff materials, to assess the feasibility and validity of the new non-standard scheme of acquisition proposed from TOTAL E&P, merged with an innovative processing technique. We extracted the Rayleigh dispersion curves (DCs) by means of an innovative multichannel method, practically our processing methodology consists in a moving square-window which slides over the acquisition array for the selection of the receivers and a moving circumference, having the same centre of the square-window, for the selection of the shots. For each position of the moving window, we obtain a local DC, therefore, the dataset to be inverted it is composed by a unit of DCs that are associated to a series of spatial coordinates, represented by the centre of each square-window. To build a 3D VS model, we invert the fundamental mode of the DCs using the Laterally Constrained Inversion (LCI) algorithm, that consist in a deterministic inversion where every 1D model is related to its neighbors with a mutual constraint to offer a single pseudo-2D or pseudo-3D model. Then, to take advantages of all the benefits of including the higher modes in the inversion, (increase the investigation depth, increase the resolution etc.), we invert them using the Maraschini-Monte Carlo inversion. This method. allows higher modes to be considered without the necessity to associate experimental data points to a specific mode. The retrieved velocities obtained from the two different approaches are in good agreement, with an average variation of 16%. Therefore, we conclude that the METIS system merged with an expeditious processing approach, is functional to build shear wave velocity models in an area characterized by stiff materials, given the reasonable and geologically appropriate results, the limit of personal involved on the ground, wise cost, HSE exposure and the acceptable amount of time required to process the data.

## **INDEX**

ACKNOWLEDGEMENTS .....	ii
ABSTRACT.....	iii
LIST OF FIGURES .....	1
LIST OF TABLES .....	4
LIST OF ACRONYMS AND SYMBOL .....	5
INTRODUCTION .....	7
1. SURFACE WAVES .....	10
1.1-MAIN PROPERTY OF SEISMIC WAVES .....	10
1.2-SURFACE WAVES METHOD .....	12
2. AQUISITION .....	14
2.1 OVERVIEW.....	14
2.2 METIS-CARPET RECORDING APPROACH.....	14
3. DATASET .....	16
4. PROCESSING.....	19
4.1 OVERVIEW.....	19
4.1.2 HIGHER MODES IDENTIFICATION .....	19
4.1.3 LATERAL VARIATION .....	20
4.2 PHASE SHIFT .....	21
4.3 PROCESS WORKFLOW .....	21
4.4.1 CLASSIC 2D MULTICHANNEL APPROACH FOR AURIGNAC .....	24
4.4.1 INNOVATIVE MULTICHANNEL APPROACH FOR AURIGNAC .....	26
5. CLUSTERING .....	31
5.1 CLUSTER OF OUR DATA .....	31
6. LATERALLY CONSTRAINED INVERSION .....	34
6.1 BACKGROUND.....	34
6.2 METHOD.....	34
6.2.1 MCI.....	35
6.3 APPLICATIO TO AURIGNAC DATA-SET.....	36
6.3.1 MCI RESULT.....	37
6.4 CONCLUSION .....	40
7. MULTI-MODAL INVERSION .....	41
7.1 OVERVIEW.....	41
7.2 MARASCHINI'S METHOD .....	42

7.3 APPLICATION TO AURIGNAC DATASET .....	42
7.3.1 MODEL SPACE.....	42
7.3.2 RESULTS.....	46
7.4 MULTIMODAL VS FUNDAMENTAL MODES INVERSION.....	50
7.5 CONCLUSION .....	51
8. COMPARISON OF THE METHODS .....	52
8.1 INTRODUCTION.....	52
8.2 GRAPHICAL ANALYSIS .....	52
8.3 QUANTITATIVE ANALYSIS .....	54
CONCLUSION.....	59
REFERENCES.....	60

# LIST OF FIGURES

Figure 1.1- Rayleigh wave propagation.....	10
Figure 1.2-Exapmle od DC .....	11
Figure 1.3-Schematic representation of geometric dispersion of Rayleigh waves: the vertical displacement associated with a short and a long wavelength (Boiero, 2009).....	11
Figure 1.4-Different modes of propagation (Socco and Strobbia, 2004).....	12
Figure 1.5-SW method (Strobbia, 2003).....	13
Figure 2.1- Synthetic modelling showing the same image quality between conventional cross-spread and carpet recording methods. ....	15
Figure 3.1--Map of France showing the location of the site.....	16
Figure 3.2--(a) Acquisition outline of the whole area, within the polygon acquisition outline of the area analyzed in this work (b)-Elevation map in which each sub data sets have flat topography, within the polygon elevation of the area analyzed in this work (Koshro Anjom, 2021). ....	17
Figure 3.3-Acquisition outline of the area of interest. ....	18
Figure 4.1-Example of the concept of lateral variation (Boiero,2009).....	20
Figure 4.2-Flowchart.....	22
Figure 4.3-Picking procedure, (a) original spectra, (b) spectra in which the maxima have been selected, (c) obtained dispersion curve. ....	23
Figure 4.4- Geometry of the selected sources and receivers.....	24
Figure 4.5-Stacked spectrum.....	24
Figure 4.6-Geometry of the selected sources and receivers, in which two different arrays have the same midpoint.....	25
Figure 4.7-Stacked spectrum, relative to the array case 1(b), and to the array case 2 (c).....	25
Figure 4.8-Comparison of the two different DCs, in red the DC relative to the spectrum (b) and in blue the DC relative to the spectrum (c) .....	25
Figure 4.9- Geometry of the selected sources and receivers using a square window, in which the shift of the window is 50 meters from a) to b), and in which the shift is 25 meters from c) to d).....	26
Figure 4.10-Stacked spectra relative to the figure 4.8 .....	27
Figure 4.11- Scheme of stacking. (a) position of the moving window $W_i$ , the shots within the circumference of radius $r$ , (b) an example of single shot spectrum, (c) stacked spectrum (d) Stacked dispersion curve. ....	28
Figure 4.12-An example of the obtained spectrum using the phase-shift method. (a) The geometry of the selected sources and receivers. (b) The stacked spectrum where the red dots show the estimated modes of surface waves, and finally (c) the plot of the picked energy maxima (dispersion curve)..	29
Figure 4.13-DCs obtained in the processing step, (a) all the fundamental modes, (b) multimodal DCs. ....	30

Figure 5.1--Dendrogram showing the cluster system of the dispersion curves, in blue the cluster A, and in red the cluster B .....	31
Figure 5.2-Fundamental modes of the DCs plotted in term of location and cluster .....	32
Figure 5.3-Dispersion curves in the seismic area .....	32
Figure 5.4-Higher modes of the DCs plotted in term of location and cluster.....	33
Figure 6.1-Flowchart LCI .....	37
Figure 6.2-Estimated VS-(a) for the reference DC of Cluster A. (b) for the reference DC of Cluster B. (Khosro Anjom, 2021), .....	37
Figure 6.3-(a) The obtained Poisson's ratio for LCI application for cluster A. (b) The estimated Poisson's ratio for cluster B in blue. The obtained Poisson's ratio for LCI for cluster B. ....	38
Figure 6.5--Horizontal sections of the estimated VS model at various depths.....	39
Figure 6.6- VS model- (a) 3D view of the obtained VS after linear interpolation of the 1D models. (b) Multiple iso-surfaces in x, y, and z directions from the 3D model. ....	39
Figure 7.1- LCI result for the high velocity area .....	43
Figure 7.2- LCI result for the low velocity area .....	43
Figure 7.3-LCI result for the high velocity area after removing outliers.....	44
Figure 7.4LCI result for the slow velocity area after removing outliers.....	44
Figure 7.5-Final boundary for the high velocity area. ....	45
Figure 7.6-Final boundary for the low velocity area. ....	45
Figure 7.7-Best fitting profile for one sample of cluster A.....	46
Figure 7.8-Absolute value of the Haskell–Thomson matrix determinant for best-fitting model of cluster A (white dots represent the experimental dispersion curve). ....	46
Figure 7.9-- Dispersion curves for best models compared with the experimental dispersion curve. ....	47
Figure 7.10-Best fitting profile for one sample of cluster B.....	47
Figure 7.11-Absolute value of the Haskell–Thomson matrix determinant for best-fitting model of cluster B (white dots represent the experimental dispersion curve). ....	48
Figure 7.12- Dispersion curves for best models compared with the experimental dispersion curve. ....	48
Figure 7.13-VS model (a) 3D view of the obtained VS after linear interpolation of the 1D models. (b) Multiple iso-surfaces in x, y, and z directions from the 3D model.....	49
Figure 7.14-Comparison of the inversions (a) result of the inversion considering only the fundamental mode, (b) the result of the inversion also considering the higher modes.....	50
Figure 8.1- The estimated VS model at a depth equal to 20 meters, (a) results from LCI, (b) results from multi-modal Monte Carlo Inversion.....	52
Figure 8.2-The estimated VS model at a depth equal to 50 meters, (a) results from LCI, (b) results from multi-modal Monte Carlo Inversion.....	53
Figure 8.3-The estimated VS model at a depth equal to 80 meters, (a) results from LCI, (b) results from multi-modal Monte Carlo Inversion.....	53

Figure 8.4-The estimated VS model at a depth equal to 100 meters, (a) results from LCI, (b) results from multi-modal Monte Carlo Inversion.....53

Figure 8.5-The estimated VS model the at a depth equal to 130 meters, (a) results from LCI, (b) results from multi-modal Monte Carlo Inversion.....54

Figure 8.6-Variation of VS model at a depth equal to 20 meters, (a) variation in terms of (m/s), (b) variation in terms of (%) .....56

Figure 8.7-Variation of VS model at a depth equal to 50 meters, (a) variation in terms of (m/s), (b) variation in terms of (%) .....57

Figure 8.8-Variation of VS model at a depth equal to 80 meters, (a) variation in terms of (m/s), (b) variation in terms of (%) .....57

Figure 8.9-Variation of VS model at a depth equal to 20 meters, (a) variation in terms of (m/s), (b) variation in terms of (%) .....57

Figure 8.10-Variation of VS model at a depth equal to 130 meters, (a) variation in terms of (m/s), (b) variation in terms of (%) .....58

## LIST OF TABLES

Table 3.1- Acquisition parameters for the whole dataset.....	16
Table 6.1-Model's parameters .....	38
Table 8.1-Variation of the VS result of the higher modes in comparison with the result of the fundamental modes .....	55
Table 8.2-Variation in percentage of the VS result of the higher modes in comparison with the result of the fundamental modes .....	56

## LIST OF ACRONYMS AND SYMBOL

DART	Downfall Air Receiver Technology
DC	Dispersion curve
F	Frequency
FDTD	Finite difference time domain
GPS	Global positioning system
HSE	Health safety environment
IoT	Internet of things
K	Wavenumber
LCI	Laterally constrained inversion
m	Model
MASW	Multichannel analysis of surface waves
MCI	Monte Carlo Inversion
p	Slowness
r	Radius
RT	Real time
SDC	Stacked dispersion curve
S(m)	Misfit function
SPAC	SPatial AutoCorrelation
SW	Surface Wave
SWM	Surface Wave methods
S-wave	Surface Wave
T	System matrix
v	Phase velocity
VS	Shear wave velocity

VP	Primary wave velocity
W	Window
W/D	Wavelength Depth relationship
$\Delta W$	Shift of the spatial windows
$\nu$	Poisson's ratio
1D	One-dimensional
2D	Two-dimensional
3D	Three-dimensional

# INTRODUCTION

Surface Wave methods (SWM) are well-established to retrieve S-wave velocity (VS) models for stratified media (Socco et al. 2010). In surface wave methods, usually the surface wave dispersion is exploited and used to estimate local VS models. The local VS models then can be used to build 2-D and 3-D velocity models considering lateral interpolation.

Since the phase velocities of surface wave are dispersive, in the analysis of surface wave, the experimental data are analyzed to retrieve the dispersion curve (DC - phase velocity as a function of frequency) which is used to solve the inverse problem. Then, the DCs are inverted to find the VS model.

One of the most interesting area to be investigated, with the SWM, are the foothills environment, this is because significant amount of hydrocarbon and mineral resources are believed to be located in this hard to access area. But, the main issue is that in those areas logistics are so costly and by employing the classic acquisition approach the obtained data are often not valuable. This is the reason why those areas cannot be examined by using conventional seismic methods, this pave the way for the development of new technologies to find the possibilities to investigate those areas by rethinking geophysical acquisition: IoT, drones, or artificial intelligence are few examples (Rassenfoss, 2017). An interesting example of the use of drone for an innovative seismic acquisition is presented in Masoni et all (2019), another relevant example is the work of Blacquiere and Nakayama (2019) in which is explained the use of artificial intelligence for an optimum seismic acquisition.

The METIS project, launched by Total EandP and partners, basically is a new disruptive onshore acquisition method which simplifies the acquisition in remote areas such as foothills. The target of this project is to develop an innovative approach for the foothills seismic acquisition survey by employ a wireless real-time seismic receiver array combined with an innovative deployment of the array by Unmanned Aerial Vehicles, this innovative method unlocks the opportunity to explore acreage in hard-to-access onshore areas and at the same time limits the number of personal involved on the ground and keeps cost and HSE exposure to a minimum (Puntous et all, 2018)

Essentially, the goal of the METIS operational model is to ensure the seismic data quality by deploying a very dense grid of seismic sensors (basically, one every 50 meters), this technique is known as “carpet recording” because it “carpets” the pavement in the exploration area, by means of DART wireless geophysical sensors which are dart-shaped. (Pierre-Olivier Lys and the METIS Team, Total 2018).

The favored method for the determination of near-surface S-wave velocity structure is the multichannel analysis of surface waves (MASW) (e.g., Miller et al., 1999; Song et al., 1989; Xia et al., 1999). This method introduced by Park et al. (1999), as a nondestructive test, time by time became more popular because of its large range of applications and benefits (Banab and Motazedian, 2010). The efficiency of this approach has been demonstrated by oil exploration industries over the last decades (Chon Park et all, 2001). Exhaustive advancement process and case study of high-frequency Rayleigh-waves technique have been summarized by Socco et al. (2010) and Xia et al. (2009). The main reasons by which the multichannel approach should be selected are that: it averages and attenuate errors (Park et al., 1999; Xia et al., 2002), enhances the mode separation and recognition (Park et al., 1998; Xia et al., 2003), permits to filter coherent noise and does not necessitate convoluted acquisition methods to sample the propagation over an adequate frequency band (Socco and Strobbia 2004).

One of the issues of this approach is that the number of geophones used, the length of the receiver spread, the receiver spacing and the source offset, can affect the quality of the multichannel surface wave records that are obtained (Park et al., 2001, 2002; Park and Carnevale, 2010). Another important aspect is that in the case of full 3D acquisition scheme, in which there is an irregular grid of sources and receiver the classic multichannel approach does not offer valuable results because become problematic the selection of different array. For this reason, most of the examples of using the MASW technique are concentrated on 2D models or data from a 1D linear receiver spread, but time to time some authors proposed application of this method also for 3D data. A 3D method was developed by Lee and Ross (2008) to mitigate surface-wave noise in spatially inhomogeneous media, Boiero and Socco. (2011) developed a method to estimate surface-wave dispersion curves from 3D seismic acquisition, based on the analysis in the offset domain and the  $f$ - $k$  multiple signal classification transforms, Wang et al (2015) expanded the finite difference time domain (FDTD) scheme of Wang et al. (2012) from 2D to 3D. Following those examples, we apply some change to the classic multichannel approach to investigate a 3D dataset.

Another important aspect, when we deal with the surface waves analysis, is relative to the inversion. Since surface wave propagation is a multimodal phenomenon (Socco et al., 2010), the DC is composed by several modal curves, but in surface wave analysis often only the fundamental mode is considered. Many authors explained the importance and the advantages of including the higher modes, in particular, in numerous cases, the experimental DC is the product of the superposition of numerous modes (Socco et al., 2010). Additionally, considering the higher modes in the inversion step can increase the precision of the result (Ernst, 2008; Maraschini et al., 2008), because they are responsive to parameters to which the fundamental mode is weakly affected (Socco and Strobbia, 2004), moreover, in the case of a velocity decrease with depth (Gucunski and Woods, 1992; Xia et al., 2003). considering higher modes can rise the investigation depth (Gabriels et al., 1987) and when the low-frequency band is not accessible (Ernst, 2008), can stabilize the inversion process (Xu et al., 2006), and can augment the resolution of the inverted model (Socco and Strobbia, 2004).

In this thesis, we want to evaluate the feasibility and validity of the new non-standard scheme of acquisition proposed from TOTAL, merged with an innovative processing technique, multichannel approach with some small change, for the inversion of the single fundamental modes and the inversion of the higher modes, to define a VS model. To do this we propose an application to a dataset acquired in a mining site in the province of Aurignac, south France, characterized by stiff materials.

Briefly, the structure of this thesis can be divided as follow:

- At first, we present the main features of the seismic waves.
- Secondly, will be introduce an innovative multi-channel approach (usually array of receivers are lined up in an equally spaced line on the test site, and the surface waves are generated by impulsive or vibrating seismic sources that are applied at one end of the receiver line-up, but in the case of a full 3D acquisition scheme of irregular geometry of sources and receivers this creates mistakes and problems in the interpretation of the results, to overpass this issue we modify the classic linear approach using a so-called square multichannel),
- Thirdly, to consider the laterally topographic variation in the analyzed area and to build a 3D VS model, we will present the inversion of the fundamental single mode of a set of dispersion curves using the Laterally Constrained Inversion (LCI) algorithm, a deterministic inversion in which each 1D model is linked to its neighbors with a mutual constraint to provide a single pseudo-2D model (Socco et al., 2010),

- Then, to avoid mode-misidentification errors in the retrieved velocity profiles and to reduce the computational cost we will present the inversion including the higher modes using the Maraschini-Monte Carlo inversion, method centered on a misfit function for multimodal inversion, based on the Haskell-Thomson matrix method, that allows higher modes to be considered without the need to associate experimental data points to a specific mode.
- At the end, will be presented the comparison of the obtained results.

# 1. SURFACE WAVES

In this section the most important characteristic of Seismic Waves propagation, in particular Rayleigh waves, are outlined to point out the aspects that are relevant for constructing a subsurface S-wave velocity model. Then, a concise summary of the operation workflow used to build the VS model will be presented, to allow the reader to comprehend the role of each step (acquisition, processing and inversion) of the method.

## 1.1-MAIN PROPERTY OF SEISMIC WAVES

SWs propagate parallel to the Earth's surface and decay exponentially in depth (Figure 1.1).

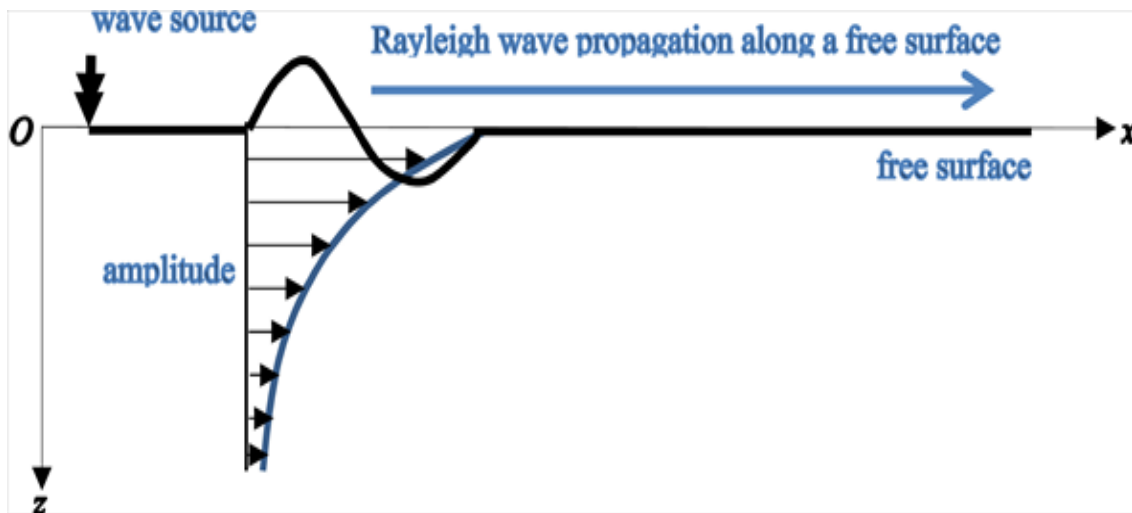


Figure 1.1- Rayleigh wave propagation

In the case of homogeneous linear elastic isotropic media, the maximum energy related to Rayleigh wave propagations travels at a depth of about one time the wavelength. Moreover, when the seismic source is situated at the surface or near the surface, SWs are more energetic than body waves (Richart et al., 1970). As well, considering that they do not spread energy in all directions (Aki and Richards, 2002), their attenuation is slower than the attenuation of body waves that spread energy in depth. This is one of the reasons why SWs are dominant events in seismic records, in particular, at far offset.

On the other hand, considering that the harmonics of a propagating SW have diverse wavelengths that propagate with different maximum depths, in a vertically heterogeneous medium the propagation of surface waves is characterized by geometric dispersion, this means that different frequencies

propagate with different phase velocities, the relation between frequencies and phase velocities is called dispersion curve (Figure 1.2).

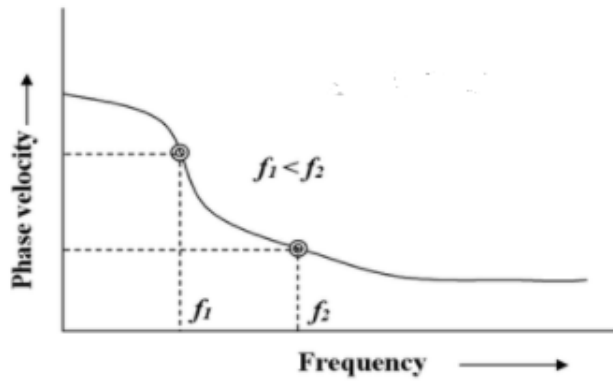


Figure 1.2-Example of DC

Considering the above considerations, the SW propagation is affected only by the mechanical and geometric properties of the part of subsoil in which they propagate. In particular, the high frequencies (short waves) propagate in top layers and as a consequence their velocity is function of the shallow soil properties, in contrast, the low frequencies (long wavelengths) propagate in thicker layers and their velocity is affected also by the characteristic of deeper layers (Socco and Strobbia, 2004), as it is shown in Figure 1.3b.

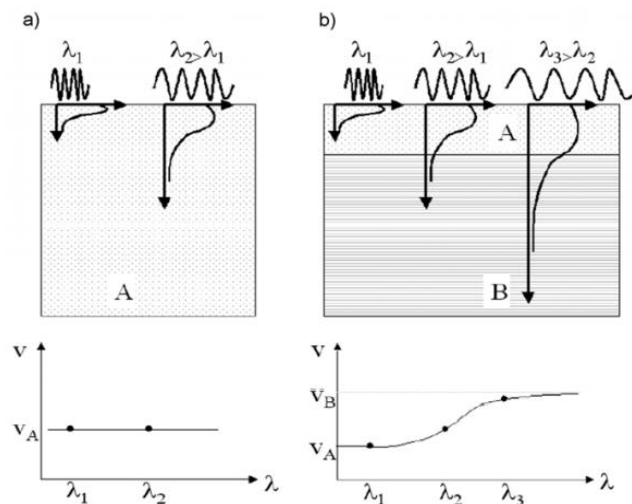


Figure 1.3-Schematic representation of geometric dispersion of Rayleigh waves: the vertical displacement associated with a short and a long wavelength (Boiero, 2009).

Another important aspect of S-waves is that in vertically heterogeneous media the propagation is a multimode phenomenon, that means that at the same frequency different velocities of propagation can exist (Figure 1.4).

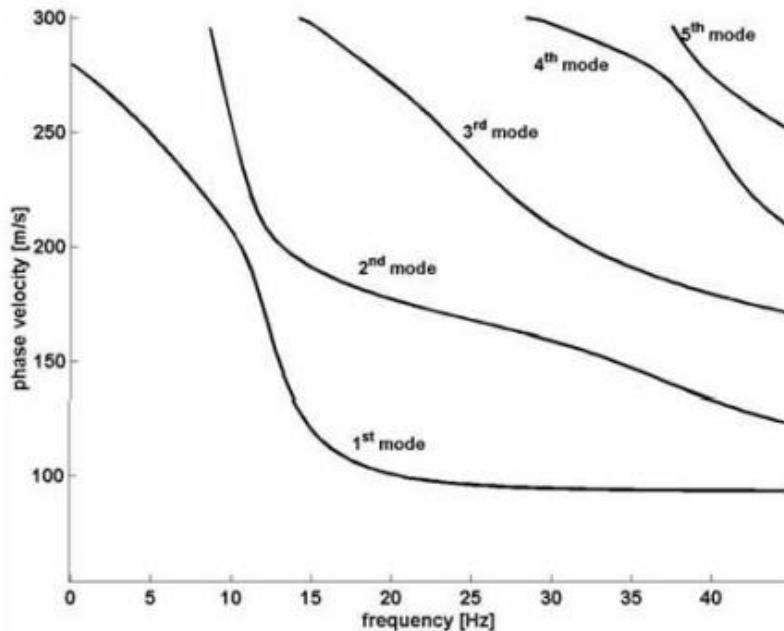


Figure 1.4-Different modes of propagation (Socco and Strobbia, 2004).

In heterogeneous media, often the fundamental mode (the slowest one) is the most energetic, but sometimes higher modes are detectable, and they can be used in the inversion process to increase resolution and investigation depth.

## 1.2-SURFACE WAVES METHOD

By analysing SW geometrical dispersion it is possible to retrieve information about the SV-wave velocity of the subsurface down to a depth that depends on the propagating wavelengths. The SW method can be summarised in three main steps (Figure 1.5):

1. Acquisition
2. Processing
3. Inversion

The acquisition consists in recording seismic data containing SW with high signal to noise ratio and in a broad frequency band. The processing involves extracting the information about the dispersion

characteristics of SWs, i.e. the experimental dispersion curve, from seismic records, and the inversion uses it to estimate the model parameters.

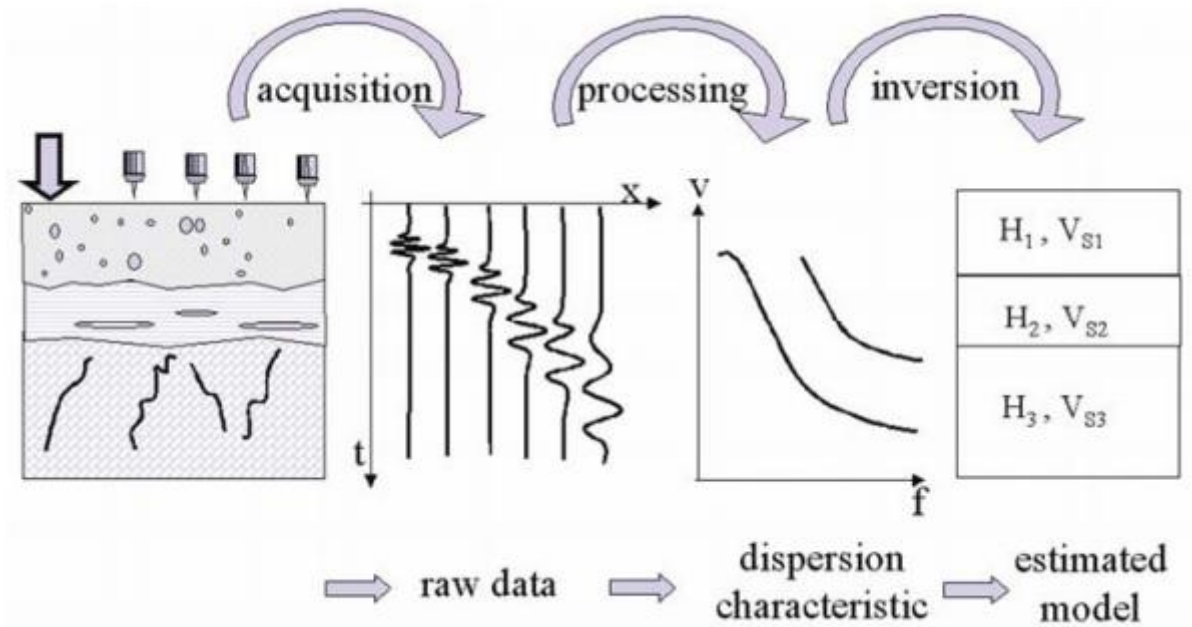


Figure 1.5-SW method (Strobbia, 2003).

In the following chapters, we will present an innovative acquisition technique (carpet acquisition), used to retrieve the seismic data used in our case study, the processing applied to the data and, finally the result of the inversion.

## **2. AQUISITION**

### **2.1 OVERVIEW**

Depending on the type of application, on the depth of investigation and on the scale of acquisition, there are different acquisition techniques that can be used in surface-wave testing. Essentially, it is possible to extract surface-wave dispersion curves from active and passive data.

When the acquisition is performed on purpose the benefit is that it is possible to choose the optimal equipment and testing setup, moreover it is interesting to notice that data sets acquired for body-wave analysis, even though not specifically designed for surface-wave analysis, often are rich in surface waves that can be processed along with body waves with significant synergy (Foti et al., 2003; Yilmaz et al., 2006; Socco et al., 2008).

The ideal data to be processed and inverted should have a high signal to noise ratio over a broad frequency band, should permit for modal separation and recognition, should allow for separating and filtering out of coherent noise, and should allow estimation of uncertainties (Socco and Strobba, 2004).

A significant amount of hydrocarbon resources is believed to be located in hard-to access onshore areas, like foothills. Often, conventional acquisition techniques for the exploration of those areas result expensive, computationally costly and with an elevated environment impact, and for those reasons they are underexplored. To overcome those difficulties new technologies have developed, and thus have opened new horizons and innovative ways to rethink geophysical acquisition: IoT, drones or artificial intelligence are only a few examples of these innovations (Rassenfoss, 2017).

### **2.2 METIS-CARPET RECORDING APPROACH**

To solve major issues for oil and gas exploration related to geophysical imaging in areas of complex topography, in the recent years, Total E&P has concentrated efforts on major advance technologies to improve the quality of the acquisition in hard to access area. In particular, the company has embarked an integrated geophysics and logistics R&D project called METIS, Multiphysics Exploration Technology Integrated System (Lys et al., 2018; Puntous et al., 2018; Pagliccia et al., 2018).

METIS introduced a new acquisition method, based on an irregular carpet of receivers which are deployed over the exploration area by means of DART wireless geophysical sensors dropped using drone swarms.

It consists of deploying a dense grid, of seismic sensors and presents the double advantage of finely sampling the upcoming wave field, while limiting the number of seismic sources required to illuminate the subsurface. Indeed, in complex areas like foothills or jungle environments, seismic sources are more costly, dangerous, and damaging to the environment than deploying additional receivers. The sources themselves will be spread over a loose grid based on logistic constraints (existing roads) .

In Figure 2.1 (Lys et al., 2018), we show the METIS operational model, the carpet recording replaces the common conventional cross-spread acquisition scheme.

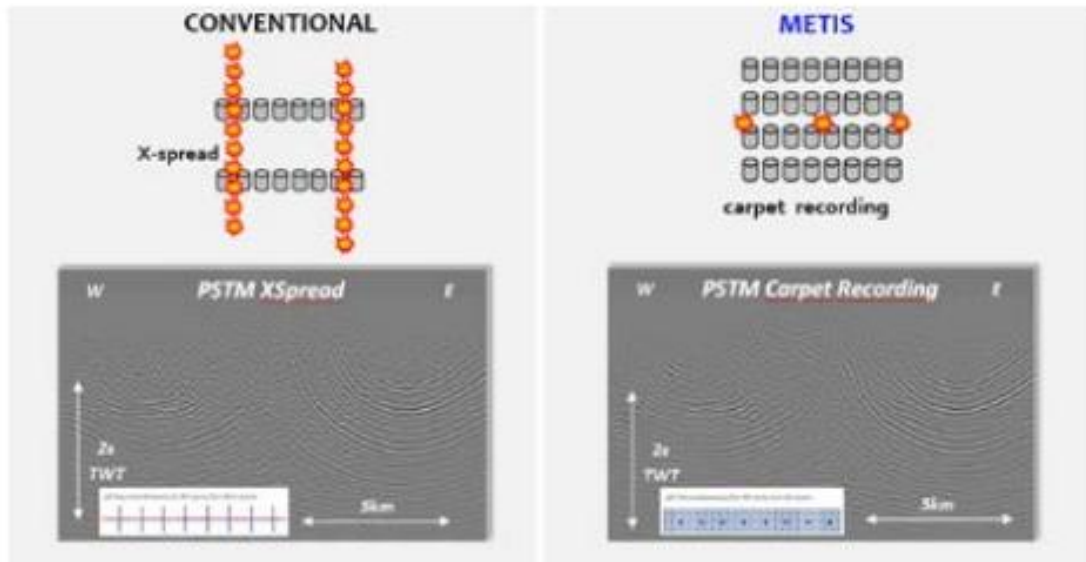


Figure 2.1- Synthetic modelling showing the same image quality between conventional cross-spread and carpet recording methods.

The target of METIS is not only to innovate the acquisition techniques but also to innovate the processing techniques, this means that the final aim, is to test the potentiality of the surface waves techniques for building shear wave velocity models from dataset acquired employing the carpet acquisition scheme.

In this contest there is a scientific collaboration between Total E&P and Politecnico di Torino. For this reason, various dataset acquired from Total E&P have been analyzed. It is important to underline that the dataset are acquired adopting the carpet geometry, in some cases using the METIS system based on drone and in other cases without the using of drone.

An analysis on a dataset acquired without using drones, but with a comparable geometry that could be obtained by using the METIS approach, will be presented in the next chapters.

### 3. DATASET

The seismic data were acquired in a mining site in the province of Aurignac, south France (Figure 3.1). The acquisition was performed inside and outside the two active open mining pits. Here, we analyze the North West portion of the dataset. The aim of our analysis is to estimate the VS model.



Figure 3.1--Map of France showing the location of the site

The dataset was acquired using several types of sources (vibrator truck, electromagnetic sources, and weight drop) but after analyzing the records we concluded that the data from the vibrator truck were the most promising for the surface wave applications. The selected source was the Birdwagen Mark IV off-road trucks equipped with a 24-ton vibrator. The recording system was a RT2, 5 Hz wireless, vertical, receiver system, this allows to record the data remotely. The topographic survey was carried out with real-time kinematic GPS system, with 0.01 m accuracy. The description of the acquisition parameters is given in Table 3.1. For more details about the acquisition parameters, it is possible to refer to Khosro Anjom, (2021).

Table 3.1- Acquisition parameters for the whole dataset.

RECEIVERS	SOURCES	NUMBER OF RECEIVERS	NUMBER OF SHOTS	SAMPLING RATE [ms]	RECORDING TIME WINDOW [s]
5 Hz geophones	Vibroseis truck	217 (spacing 25 to 50 m)	182 (irregular layout)	2	5

The site is characterized by stiff material, and this makes the surface wave analysis challenging, moreover, the topography produces distortion in the propagation of surface wave. To lessen the effect of the topography, the dataset was divided into four sub datasets, each with relatively flat topography. In Figure 2.2a the map of the area is shown, where the triangles are the receiver positions and the “+” are the source locations. Each sub dataset is depicted with a distinct color. The data set in the North-west used in this thesis is highlighted by the white polygon. In Figure 2.2b it is shown the elevation map of the whole area, again with a polygon that underlines the area of interest.

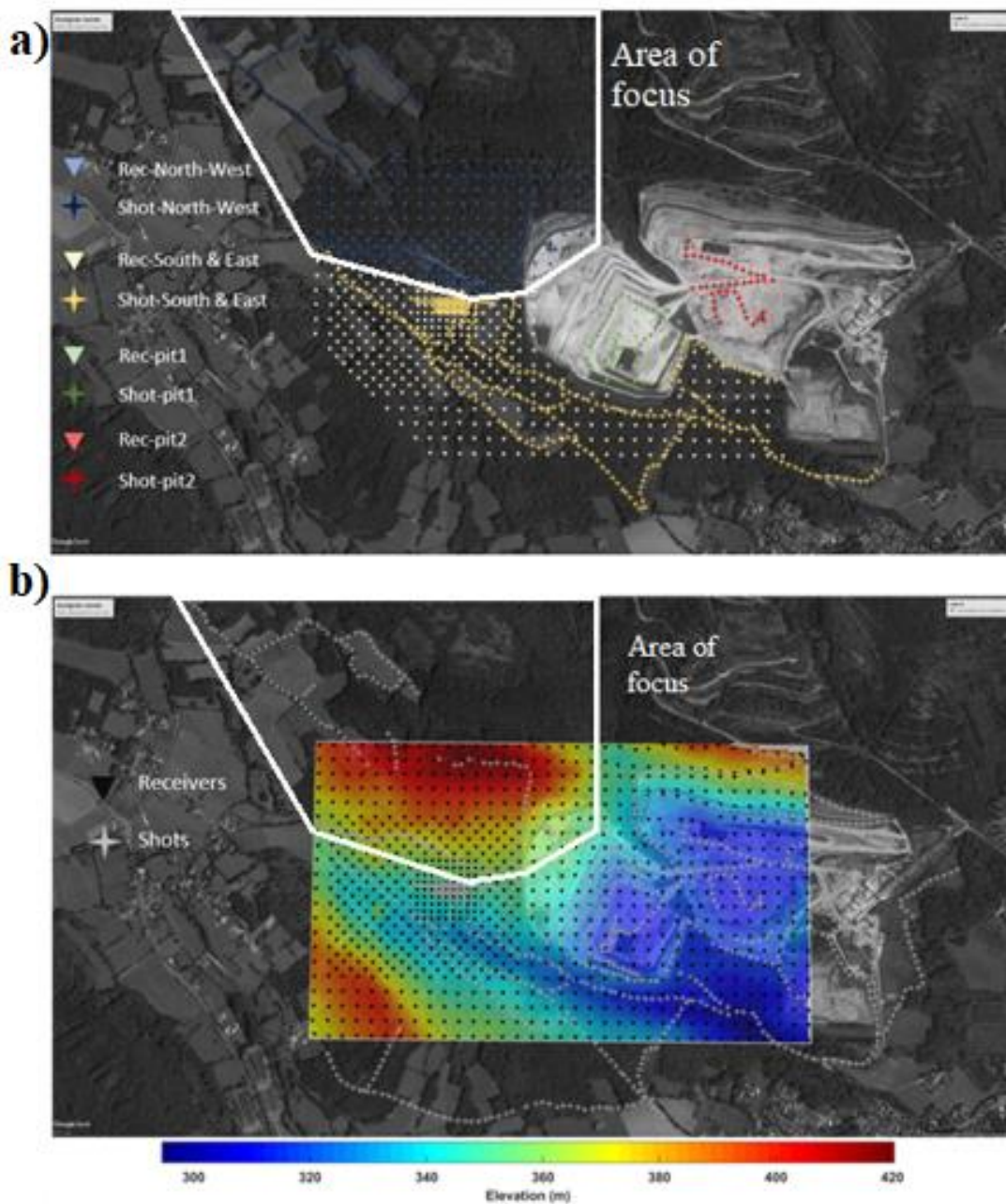


Figure 3.2--(a) Acquisition outline of the whole area, within the polygon acquisition outline of the area analyzed in this work (b)-Elevation map in which each sub data sets have flat topography, within the polygon elevation of the area analyzed in this work (Koshro Anjom, 2021).



## 4. PROCESSING

The task of the processing is to process the field data to estimate an experimental DC. Through time, many processing techniques have been developed but among all of them is not possible to define one as the best technique.

Most of them working in the spectral domain.

### 4.1 OVERVIEW

It is possible to distinguish different processing approaches depending on the characteristics of the data that have to be analyzed. Specific methods have been designed for active source data and passive source data. In both the cases, the best choice is to select procedures that can be applied to provide an automated extraction of the DCs.

For the analysis of active-source data, the most common approaches are transform-based methods (frequency–wavenumber (f–k), frequency–slowness (f–p) or frequency- phase velocity analysis (f–v)). The general procedure is centered on the computation of the spectra and the picking of the amplitude maxima. The data gathered in the time–offset domain are transformed to various domains where the peaks of the amplitude spectrum are observed in correspondence of pairs of wave propagation parameters (Foti et al, 2018).

In the case of passive-source data, the usual approaches are f–k analysis and SPatial AutoCorrelation (SPAC). The dispersion characteristics are obtained from statistics computed on a huge quantity of small-time blocks obtained from the long duration recorded signals (Foti et al, 2018).

Generally, the common processing approach does not take into account the lateral variations. In this thesis, the area investigated for our case study, it is characterized by lateral heterogeneities and since we want to extract numerous curves with high quality containing higher modes, we use the phase shift method because it permits to take into account the lateral variation and offer results with a good resolution.

In the following will be explained the importance of identifying the higher modes, the concept of lateral variation, and will be presented a brief overview of the phase shift method. Consequentially will be presented our approach and the relative results.

#### 4.1.2 HIGHER MODES IDENTIFICATION

An important aspect during the processing step is the proper recognition of various modes: it is required to pick the relative maxima of the spectrum and to relate them to the fundamental or to a specified higher mode. The examination and the consequent selection of each mode is manual and it is based on visual inspection of the spectrum; after that the DC is automatically recognized (Foti et al, 2018).

An issue to consider is the recognition of the mode number for every data point. This means that since part of the apparent DC could arise from the superposition of modes, some modes could be misidentified in the experimental data set.

Even if, often it is not possible to identify unmistakably the various modes, they are very useful because including the higher modes can increase the investigation depth and the resolution. Moreover, the joint use of higher modes improves the outcome of inversion in comparison with the use of fundamental mode only (Pan et al, 2019), for this reason the effort of extracting higher modes in the processing it is worthwhile.

The common difficulties in recognize the higher modes are caused by the fact that the energy distribution between the different modes may not be constant across the whole frequency band. This is caused by the velocity and attenuation structures, source characteristics and lateral variation (Foti et al, 2018).

### 4.1.3 LATERAL VARIATION

During processing it is necessary to consider the presence of lateral variation (Figure 4.1), because respect to the three main parts in which the surface wave method can be split (acquisition, processing and inversion), the presence of lateral heterogeneities in the investigated subsurface volume influences more the processing step and have also affects on the inversion. The lateral variations are responsible to alter the wave propagation and the phase velocity (Hashemi et al, 2020).

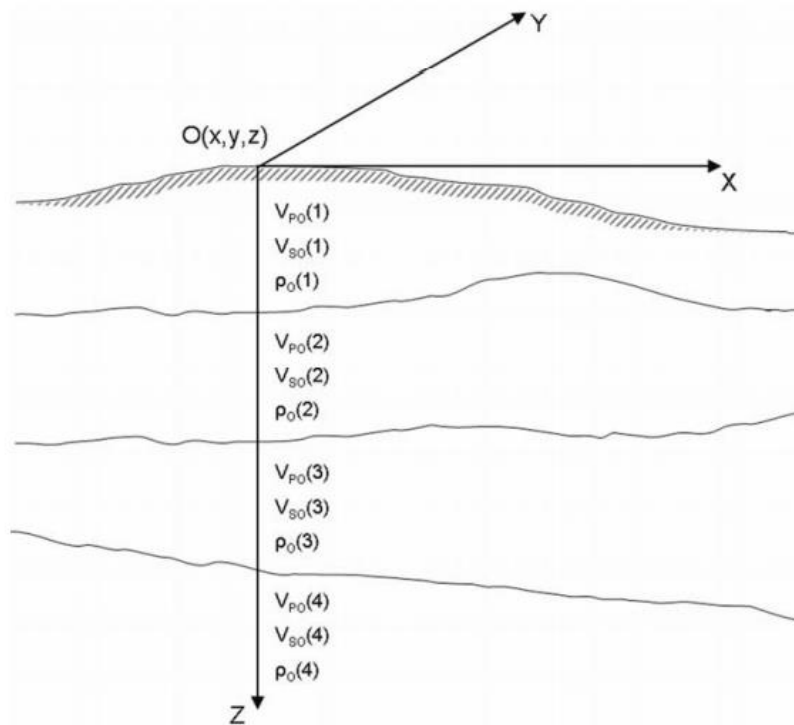


Figure 4.1-Example of the concept of lateral variation (Boiero,2009).

When we extract one DC from a set of receivers, we delete the information about the lateral variation. Moreover, during the inversion the DC will be associated to a 1D model, this means that the lateral variations are not considered. But, in the case of area characterized by lateral variations, this can generate mistake in the final VS model.

For this reason many approaches have been presented: Tian et al. (2003) expanded the spread length, Hayashi and Suzuki (2004) utilize the common mid-point (CMP) cross-correlation, Luo et al. (2007) performed the horizontal resolution analysis for a pair of synthetic traces, Socco et al. (2009) used a moving window along the receiver's line, Hashemi et al. (2019) identified subsoil lateral heterogeneities using multi-offset phase analysis of surface wave data.

## **4.2 PHASE SHIFT**

It is a method introduced by Park et al., 1998, it involves a three-step wavefield transformation that transforms surface waves on a shot gather into images of multi-mode dispersion curves. This method constructs high-resolution images of dispersion curves with relatively small number of traces.

The main advantage of this method is that it separates the different modes with higher resolution even if the shot gather consists of a relatively small number of traces collected over a limited offset range (Park et al., 1998).

In the following section of the thesis, we discuss the processing techniques procedure that we adopted for the estimation of the dispersion curves

## **4.3 PROCESS WORKFLOW**

To estimate the DCs we adopted a processing methodology consisting in a moving window, of center O, which slides over the acquisition array, so for each position we estimate a local DC that is located at the center of the window, and we considered the estimated dispersion curve as a local property of a subsoil column beneath the array

After computing the spectra through wavefield transform, we pick the energy maxima on the stacked f-v spectrum at each position of the moving window, following this approach, proposed by Grandjean and Bitri 2006; Neducza, 2007, and then suggested also in Socco et al., 2009, the signal to noise ratio it is improved through spectral stacking. In Figure 4.2 it is shown an example of picking of the energy maxima.

The technique we used it is summarized in the flowchart in Figure 4.2.

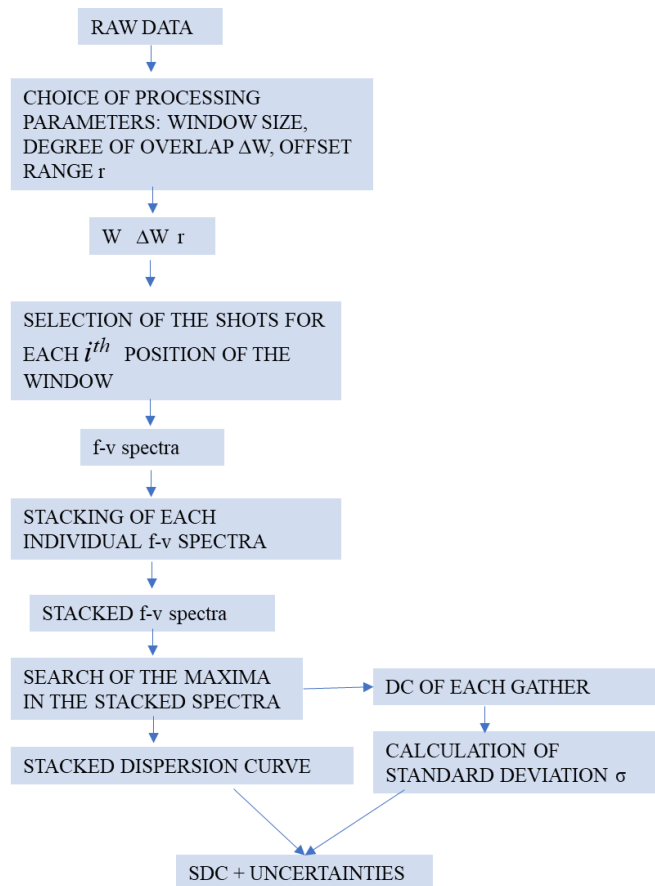


Figure 4.2-Flowchart

The first portion of the method is mainly manual and is based on tests on representative sample records, to select the processing parameters, listed below:

- size of the moving window  $W$  of center  $O$ .
- shift of the spatial windows  $\Delta W$ .
- maximum offset range  $r$  for shot selection.

To decide the optimum value of  $W$  we performed numerous tests on a few representative records. It is known that, if we want to increase the spatial resolution, we need to maintain the dimension of  $W$  as small as possible, on the other hand, to improve the spectral resolution, the window should be large enough (in terms of number of receivers) to separate the different dispersive events present in each window (Boiero, 2009).

Once the optimal processing parameters have been selected, the processing procedure is completely automatic. A group of shots is selected for each  $i^{th}$  position of the window  $W$  considering the receivers that fall in  $W_i$ . After this  $W$  is moved by increment  $\Delta W$  to the position  $W_{i+1}$ , and the process is reiterated for the whole survey area. In this way we extract a group of  $n$  dispersion curve for each  $W_i$ , where  $n$  is the number of shots that fall into  $r$ . All the individual spectra related to each shot were computed and stacked to obtain a smooth dispersion curve with higher signal-to-noise ratio

(Grandjean and Bitri, 2006; Neducza, 2007), we call the final dispersion curve obtained after stacking the “stacked dispersion curve” (SDC)

The third step is in part manual and in part automatic and consist of picking the energy maxima in the stacked dispersion curve. In particular, the maxima are searched automatically in a window that is selected manually in the spectra. An example it is show in Figure 4.3.

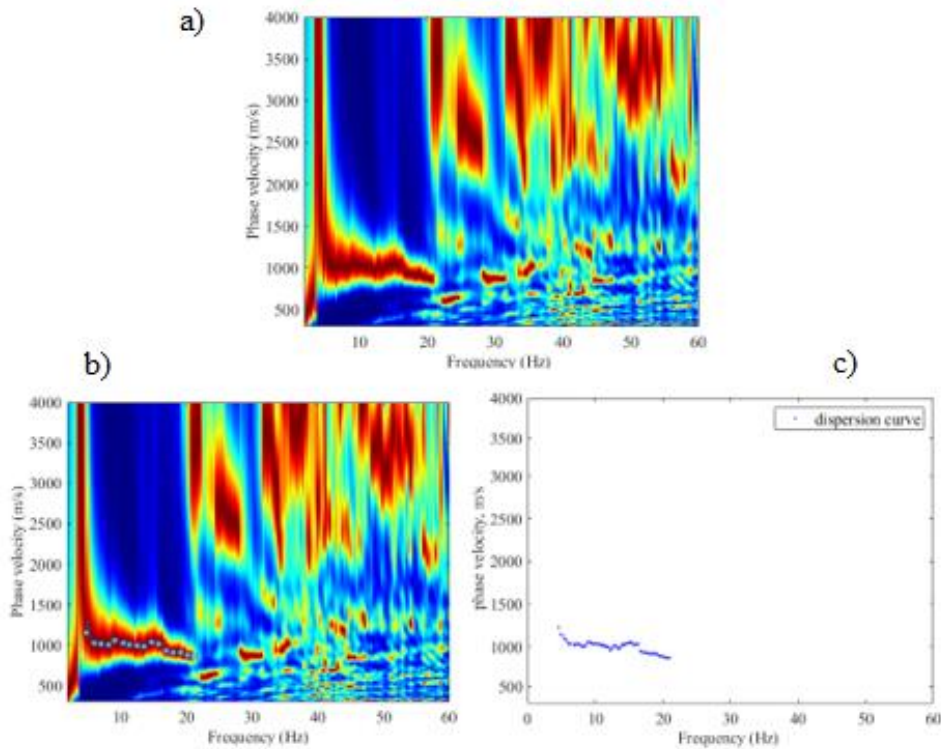


Figure 4.3-Picking procedure, (a) original spectra, (b) spectra in which the maxima have been selected, (c) obtained dispersion curve.

It is important underline that when the spectra presents also higher modes, the picking procedure is applied in different spectral zone, one for each mode.

The picking procedure is repeated for each  $W_i$  and the processing result is a set of dispersion curves, with experimental uncertainties, regularly spaced with steps  $\Delta W$  over the area, the spatial coordinates of the DCs correspond to the center of each window.

To reach this goal we tested two approaches that differ in the way by which the array and the shot have been selected. The first approach we propose is the classic 2D multichannel approach, then we propose an innovative 3D multichannel approach, in the following the results obtained will be presented and discussed.

#### 4.4.1 CLASSIC 2D MULTICHANNEL APPROACH FOR AURIGNAC

We apply the classic 2D multichannel approach, so as shown in Figure 4.4, we consider a linear array of receivers and the sources in line with it, and we attribute at the obtained dispersion curves the coordinate of the midpoint of the linear array, in this way we obtain a number of DCs, equal to the number of considered linear arrays and In Figure 4.5 it is shown an example of spectrum.

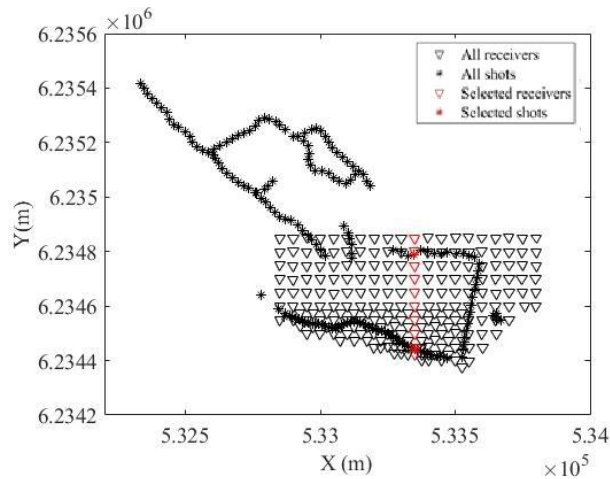


Figure 4.4- Geometry of the selected sources and receivers

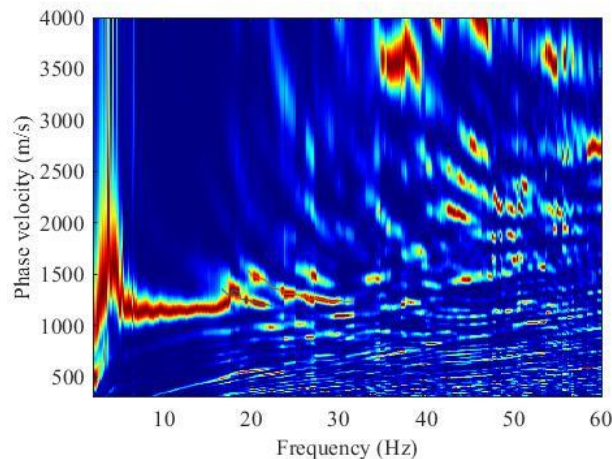


Figure 4.5-Stacked spectrum

Doing so, since we are dealing with an area characterized by lateral variation, when we consider linear array, having different azimuth, that intersects each other on their midpoint we are investigating two different zones, and as a consequence we obtain two different dispersion curves located at the same location, one example of two arrays with the same midpoint is shown in Figure 4.6 and Figure 4.7 we show the two spectra. In Figure 4.8 we show the comparison of the two obtained DCs.

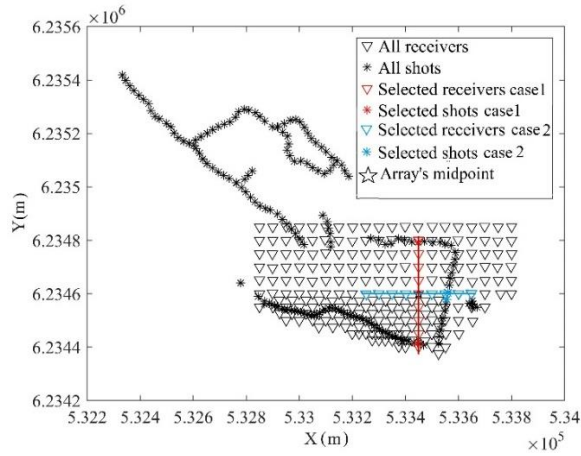


Figure 4.6-Geometry of the selected sources and receivers, in which two different arrays have the same midpoint

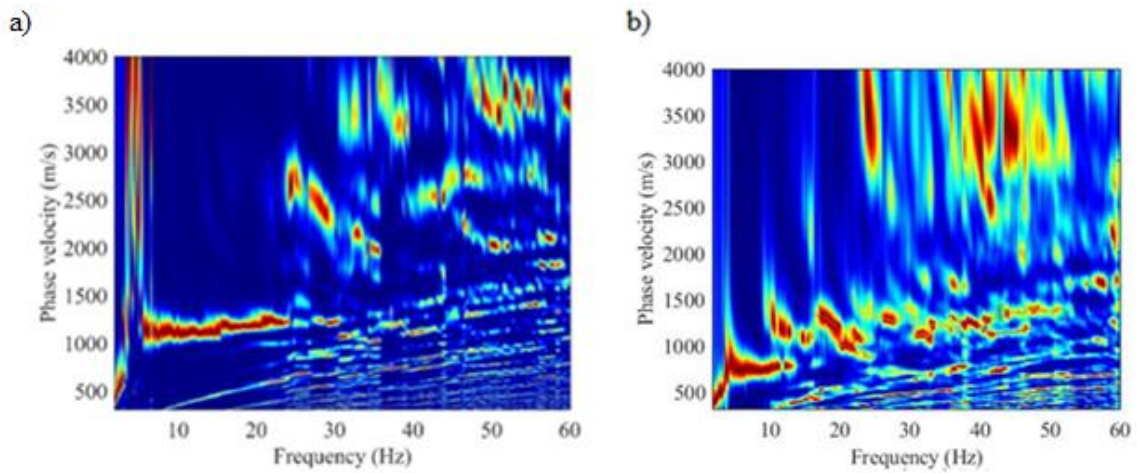


Figure 4.7-Stacked spectrum, relative to the array case 1 (b), and to the array case 2 (c)

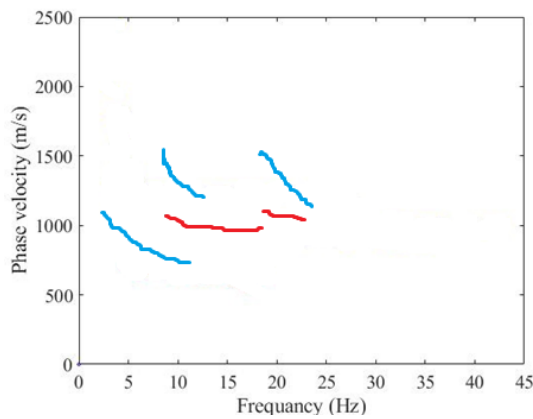


Figure 4.8-Comparison of the two different DCs, in red the DC relative to the spectrum (b) and in blue the DC relative to the spectrum (c)

As it is shown in the above Figures, although both DCs are assigned to the same location, they exhibit totally different patterns.

#### 4.4.1 INNOVATIVE MULTICHANNEL APPROACH FOR AURIGNAC

To reduce the effect of lateral variation and obtain local dispersion curves representative of the subsoil column, we adopted a processing methodology consisting in a 2D square moving window, of center O, which slides over the acquisition array.

We chose a window size equal to  $100 \times 100$  m to obtain information on a wide frequency band and to maximize the lateral resolution, moreover a condition by which the spectrum will be computed is that there are at least 8 receivers within the square window.

We also needed to select the shots to be stacked in each spatial window. We defined a circle centered in O with radius r from tests on signal-to-noise ratio, and the shots that fall within it are used, after some test we decided that the best radius to be selected was 250 meters, in this way it was possible to consider sources at different azimuth, and therefore the effects of different propagation were lessened, so the directionality had a weaker effect (Strobbia and Cassiani, 2011).

The other important parameter to be selected is the shift of the spatial window, as shown in the Figure 4.3, there are basically two areas with different receivers' density, in the North part the spacing between receivers is equal to 50 meters, and for this reason, in this area, we used a  $\Delta W$  equal to 50 meters, while for the Southern part in which the spacing between receivers is equal to 25 meters we used a  $\Delta W$  of 25 meters, in the Figure 4.9 we show some square windows in the two different subarea, and in Figure 4.10 are shown the corresponding spectra.

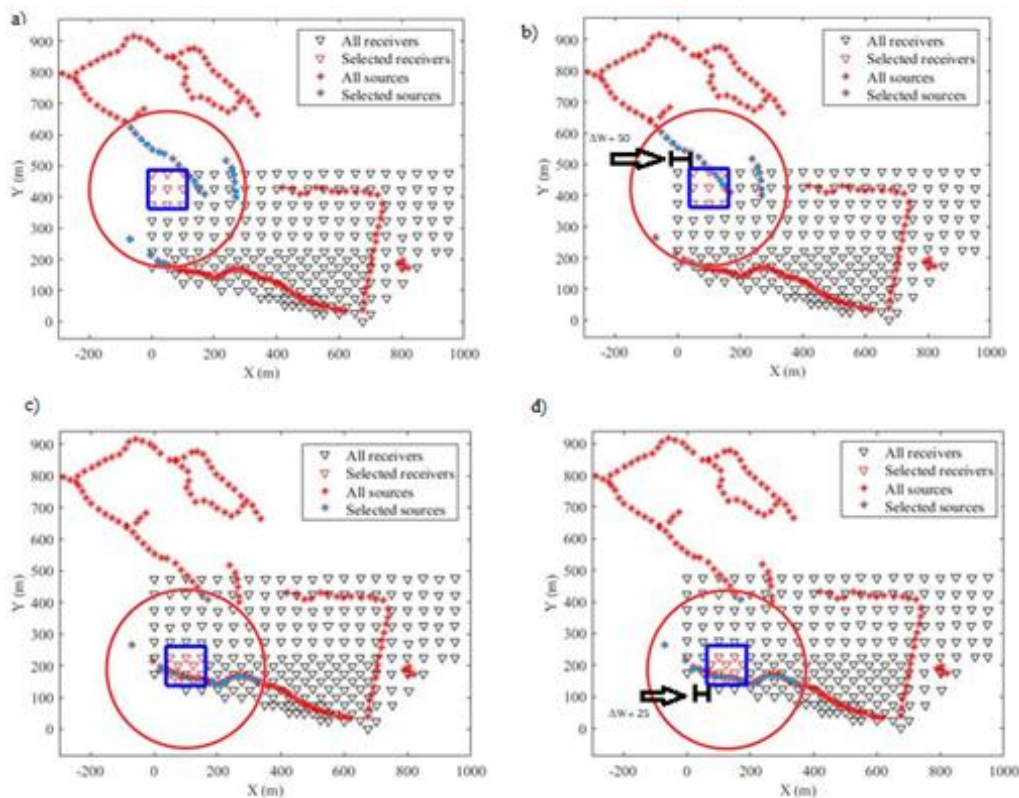


Figure 4.9- Geometry of the selected sources and receivers using a square window, in which the shift of the window is 50 meters from a) to b), and in which the shift is 25 meters from c) to d)

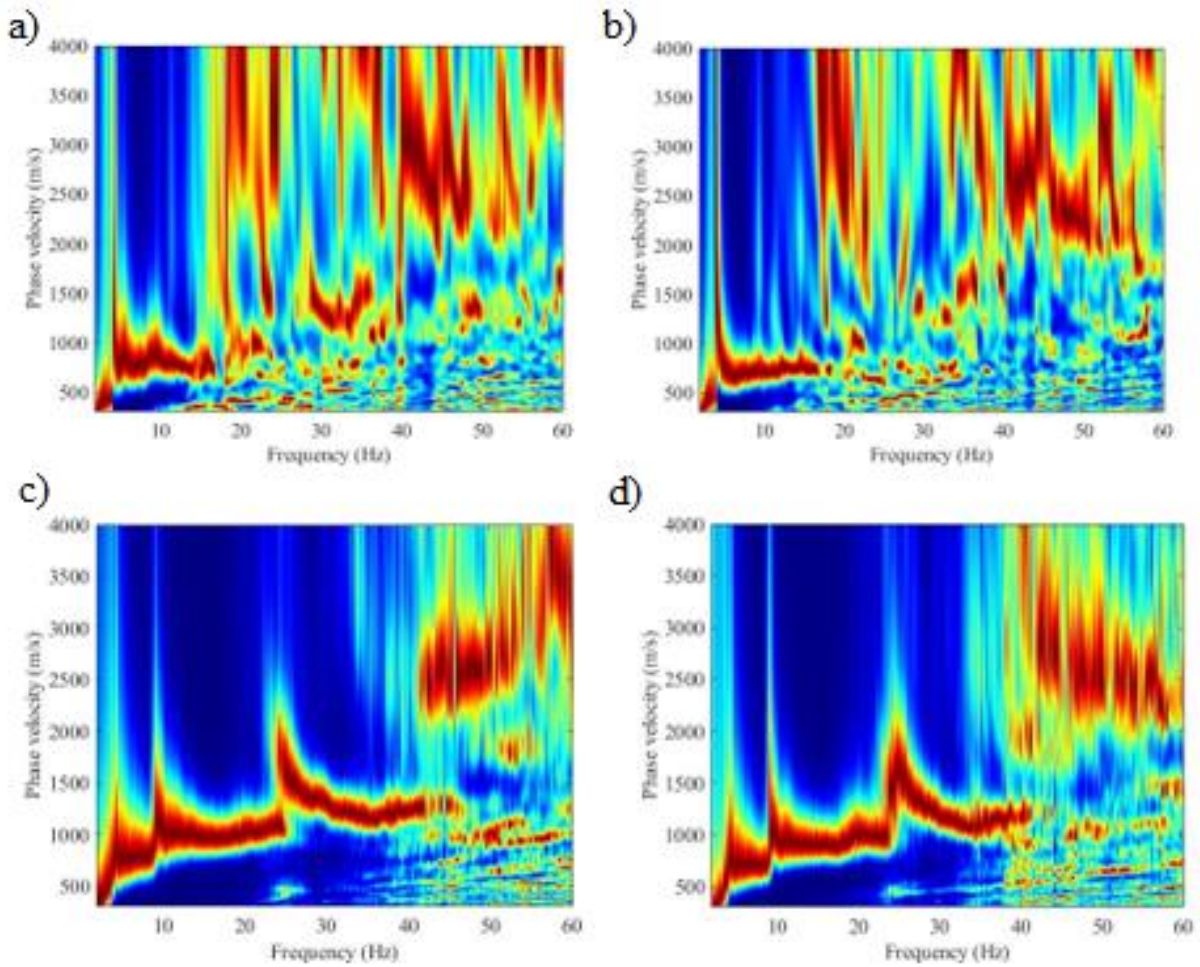


Figure 4.10-Stacked spectra relative to the figure 4.8

As already mentioned, once the optimal processing parameters have been selected, the processing procedure is completely automatic. At the end for each window  $W_i$  we obtained  $n$  individual spectra, where  $n$  is the number of shots that fall into  $r$ . All the individual spectra related to each shot, corresponding to each source within 250 m of the receiver spread, were computed and stacked to obtain a smooth dispersion curve with higher signal-to-noise ratio (Grandjean and Bitri, 2006; Neduczka, 2007), we call the final dispersion curve obtained after stacking the “stacked dispersion curve” (SDC). One example it is shown in the Figure 4.11, in which we show the spectrum of an individual shot and the stacked spectrum from all the shots within the circumference.

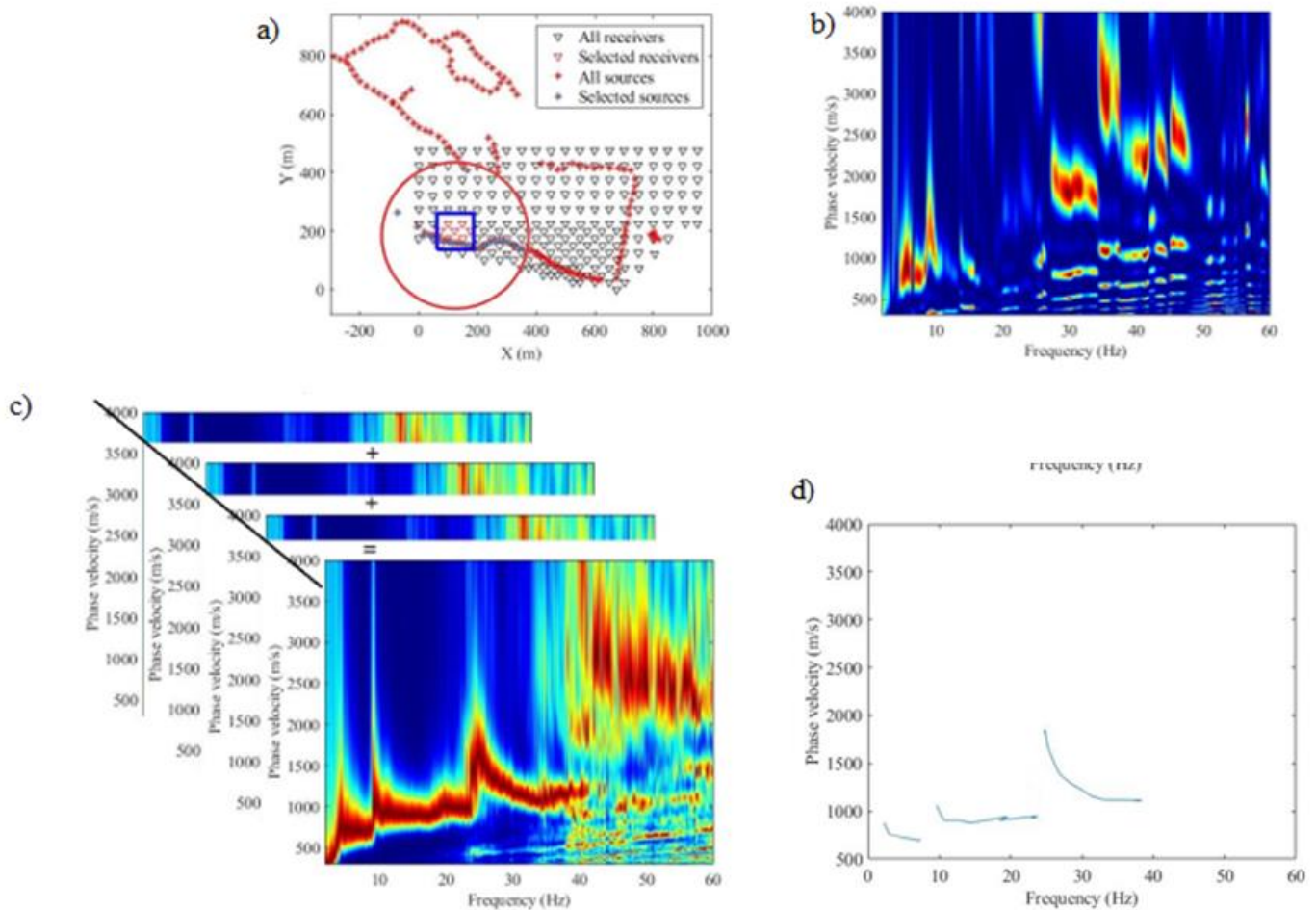


Figure 4.11- Scheme of stacking. (a) position of the moving window  $W_i$ , the shots within the circumference of radius  $r$ , (b) an example of single shot spectrum, (c) stacked spectrum (d) Stacked dispersion curve.

In Figure 4.12 we show an example of frequency vs phase velocity spectrum with the relative location of the square window and the relative DC obtained after picking the energy maxima.

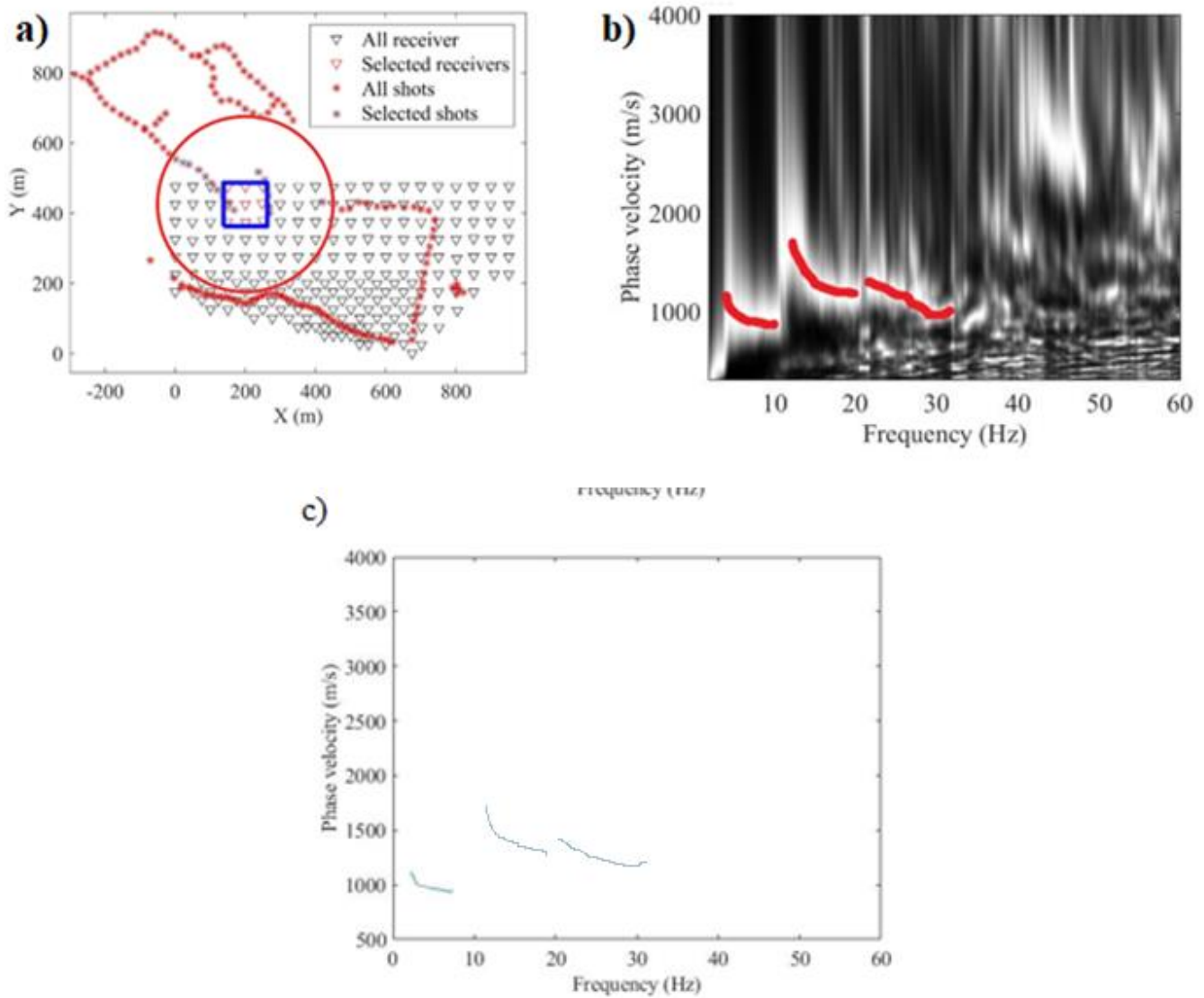


Figure 4.12-An example of the obtained spectrum using the phase-shift method. (a) The geometry of the selected sources and receivers. (b) The stacked spectrum where the red dots show the estimated modes of surface waves, and finally (c) the plot of the picked energy maxima (dispersion curve)

In Figure 4.13 we show the DCs obtained, in particular (a) all the fundamental modes and (b) the whole DCs obtained.

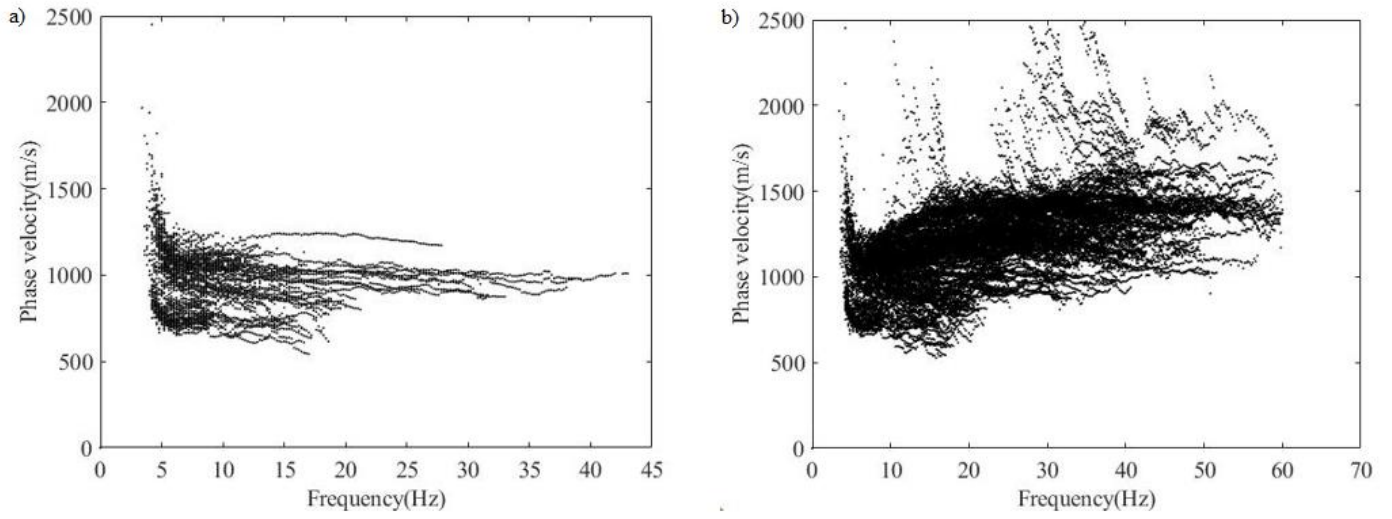


Figure 4.13-DCs obtained in the processing step, (a) all the fundamental modes, (b) multimodal DCs.

## 5. CLUSTERING

Cluster analysis or clustering is the method by which it is possible to group a set of objects in a way that components in the same group (called a cluster) are more like each other than to those in other clusters. In this work we use a hierarchical clustering method.

Hierarchical clustering also known as connectivity-based clustering consists of the principle by which objects are more related to nearby objects than to objects farther away. So practically, the procedures link "objects" to form "clusters" based on their distance. Roughly, it is possible to say that a cluster can be explained, essentially, by the highest distance necessary to link parts of the cluster. At various distances, different clusters will form, generally, they are represented using a dendrogram in which in the y-axis is plot the distance at which the clusters merge, while the objects are placed along the x-axis such that the clusters do not mix, that is why this procedure is called "hierarchical clustering". This technique does not provide a specific partitioning of the data set but provides an extensive hierarchy of clusters that merge at certain distances (Maimon and Rokach, 2000).

### 5.1 CLUSTER OF OUR DATA

Following the approach in Khosro Anjom et al. (2017) the first step of our analysis was the construction of a dendrogram, (Figure 5.1). As it is known in the horizontal axis of the dendrogram are plotted the DC numbers and in the vertical axis the distance between linked clusters. The higher the vertical nodes the further the clusters are from each other. On the dendrogram we choose the number of clusters.

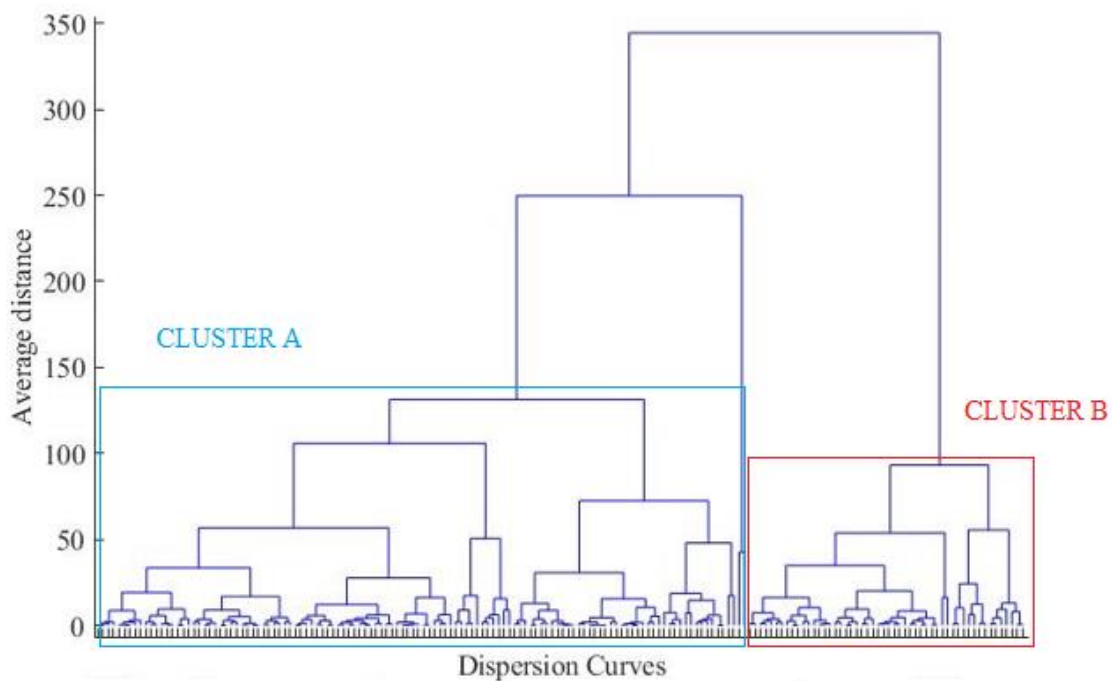


Figure 5.1--Dendrogram showing the cluster system of the dispersion curves, in blue the cluster A, and in red the cluster B

From the clustering of the 174 dispersion curves, (fundamental modes) in the dendrogram two major clusters are detected, in particular, the cluster A (represented by the blue color) composed by 123 DCs, and the cluster B (represented by the red color) composed by 51 DCs.

In Figure 5.2 we show the DCs numbered according to their position along the survey area and with different colors to indicates the clusters. The same DCs in terms of frequency, indicated with different colors based on clusters are shown in Figure 5.3 where the color indicates the clusters.

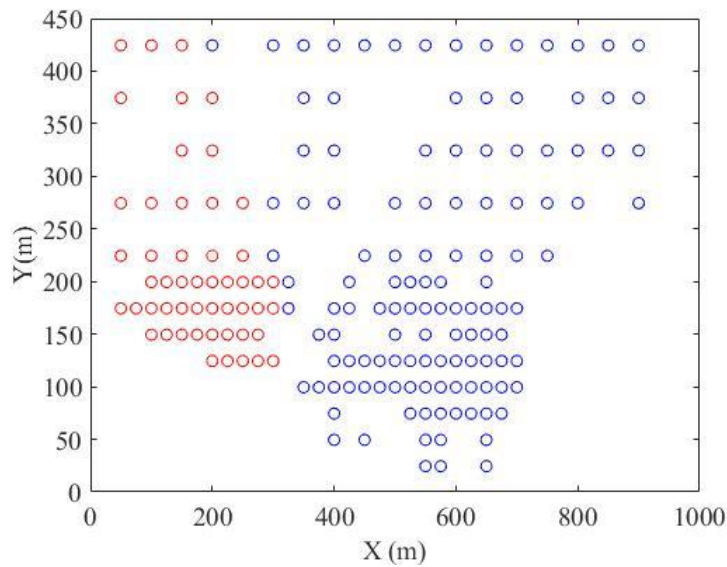


Figure 5.2-Fundamental modes of the DCs plotted in term of location and cluster

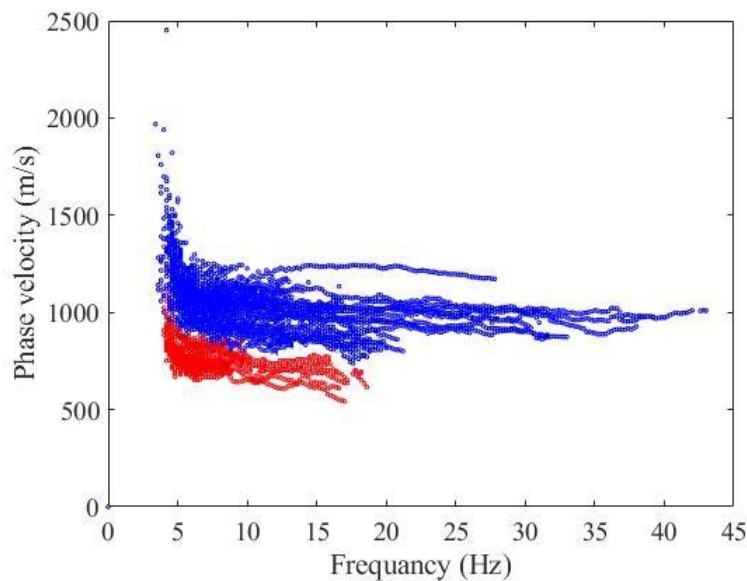
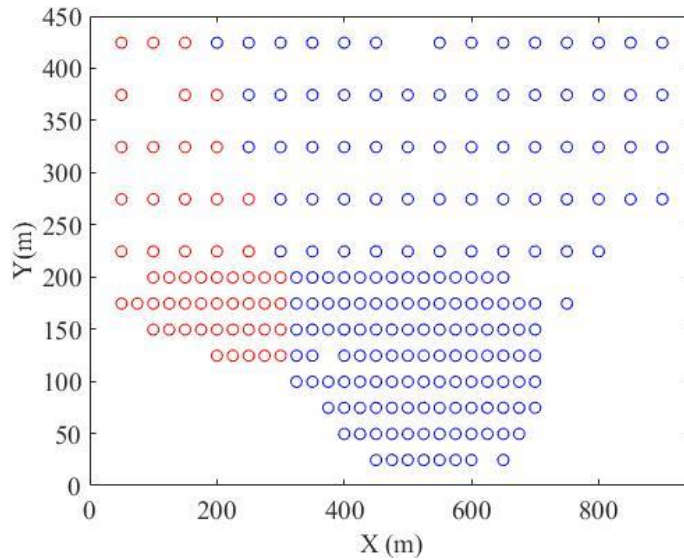


Figure 5.3-Dispersion curves in the seismic area

The clustering is very effective in identifying two different groups of DCs that correspond to different zones. This suggests that the clustering is consistent with lateral variations of the subsurface velocity. This, it is also confirmed in the clustering of the higher modes (Figure 5.4),



*Figure 5.4-Higher modes of the DCs plotted in term of location and cluster*

As already mentioned, in the case of multimodal DCs we have data almost along the whole analyzed area.

## 6. LATERALLY CONSTRAINED INVERSION

In this chapter, we describe the laterally constrained inversion (LCI) of the fundamental modes of the dispersion curves the chapter is divided in two main parts:

- the background of the adopted method by which fundamental modes are inverted
- the adopted algorithm and the relative result obtained for the used dataset.

### 6.1 BACKGROUND

The laterally constrain inversion was introduced by Auken and Christiansen, 2004 as tool for the interpretation of resistivity data. LCI, is a deterministic inversion that offers as output a single pseudo-2D/3D model, to do so every initial 1D model is related to its neighbors with a mutual constraint.

The strength of constraints is thought of as a priori information on the geological variability in the zone of interest, the higher the estimated deviation of a model parameter, the less rigid the constraint. (Socco et al., 2009).

The function of those constrains is to permit just a limited variation of each model parameter among two neighboring 1D models. The goal of the constrains and of the accessible a priori information is to make less severe the solution non-uniqueness (Shakir et all. 2013).

Numerous authors, validated the LCI method, presenting various application on resistivity and seismic data. Wisén et al. 2005 make a comparison between the LCI of 1D resistivity soundings and a 2D smoothed inversion, demonstrating that, in layered media, LCI present a superior vertical resolution. Auken et al. 2005 presented an analogous comparison for synthetic and field resistivity data with lateral variations.

The idea of LCI applied to surface wave data was initially introduced by Wisén and Christiansen 2005. Socco et all 2009 employed LCI as the last step of evaluating surface waves in seismic reflection surveys to retrieve a pseudo-2D S-wave velocity model. Boiero and Socco, 2010 display that Lateral variations can be characterized by exploiting the data redundancy of the ground roll contained in multifold seismic data, and they show that the introducing lateral constraints enhances the outcome, in comparison to individual inversions. Bardainne et al 2017 suggest a LCI of surface wave obtaining reliable near-surface shear-wave velocity field from Rayleigh wave measurements.

Here, we apply LCI for the inversion of the fundamental mode of the obtained dispersion curves. In the following, the inversion method is described and applied to the Aurignac data set.

### 6.2 METHOD

The Inversion of experimental data it is developed as a two phases process, we use a Monte Carlo Inversion (MCI) to accomplish a rigorous model parameterization and, consequently, reduce the effect of non-uniqueness of the solution. The ultimate step of this procedure consists on the LCI of local DCs to get a final pseudo 3D model.

### 6.2.1 MCI

The Surface Wave (SW) technique is centered on the inversion of surface wave DCs. The major problem of the procedure is the small sensitivity of the DC to model parameter alterations, this causes to obtained output with low-resolution and this produces an issue in defining the best model parameterization for the inversion process (Strobbia, 2009). Furthermore, another crucial feature is that the outcome may be extremely influenced by the initial model which can run the inversion into local minima, this is caused by the fact that the solution is non-unique (Luke et al., 2003). The methods that utilize a random, pseudo-random, or quasi-random succession generator to sample a parameter space are called Monte Carlo (MC) methods (Sambridge and Mosegaard, 2002; Tarantola, 2005). The reason why the MC approach is extremely attractive for the inversion of surface waves is that it precludes all the assumptions of linearity between the observables and the unknowns and additionally it offers a way of handling the non-uniqueness problem (Boiero, 2009). Practically, the MC methodology can be simple summarized as follow:

- Definition of the model parameters (number of layers, shear-wave velocity, density, Poisson ration, and thickness).
- Generation of a group of casual models.
- Computation of the synthetic DCs related to the models.
- Scaling the set of models to reduce the global distance between the experimental and theoretical curves, this operation is made artificially by shifting each of the acquired synthetic dispersion curves as close as possible to the experimental DCs by matching the curve barycenter (Socco et all, 2009).
- Invert the computed scaled model by computing the misfit among the experimental dispersion curve and the shifted DC.
- Use of a statistical test to be able to select the final models.

Doing so, the sampling is concentrated in the low-misfit regions of the model parameter space and therefore, this approach permits considerable optimization of the process by lowering the number of needed simulations (Socco et all, 2009).

### 6.2.2 LCI

This laterally constrained inversion consists on inverting simultaneously all the local DCs, minimizing a common objective function, which includes the data misfit, the a priori information, and the constraints (Auken and Christiansen, 2004).

The constraints, the a priori information, and the dispersion data are part of the inversion. Information from one model will spread to neighbouring models through the lateral constraints; the final result is a smoothly varying pseudo 2D/3D model. Consequently, the output models form a balance between the constraints, the physics and the data (Socco et all, 2009).

Model parameters with little influence on the data will be controlled by the constraints. The strength of the constraints can be considered a priori information on the geological variability in the area, the smaller the expected variation of a model parameter, the more rigid the constraint. The lateral and a priori constraints are scaled according to the model separation so that they are weakened with increased separation.

At the first step, the result of the inversion is composed of a set of 1D models, in which each model is linked to an experimental local DC. Then, the 1D models neighbor are connected sideways by lateral constraints, that claim equivalence among neighboring model parameters of equivalent typology (Boiero, 2009).

Since the SW inversion is non-linear, it is possible to write the iterative inversion scheme as the model update at the  $n$ th iteration:

$$\mathbf{m}_{n+1} = \mathbf{m}_n + \left( \begin{array}{l} \left[ \mathbf{G}^T \mathbf{C}_{obs}^{-1} \mathbf{G} + \mathbf{R}_p^T \mathbf{C}_{Rp}^{-1} \mathbf{R}_p + \lambda \mathbf{I} \right]^{-1} \times \\ \left[ \mathbf{G}^T \mathbf{C}_{obs}^{-1} (\mathbf{d}_{obs} - \mathbf{g}(\mathbf{m}_n)) + \mathbf{R}_p^T \mathbf{C}_{Rp}^{-1} (-\mathbf{R}_p \mathbf{m}_n) \right] \end{array} \right)$$

Where:

- $\mathbf{d}_{obs}$  is the local DC dataset.
- $\mathbf{C}_{obs}$  represent the observational covariance matrix.
- $\mathbf{G}$  is the sensitivities matrix.
- $\mathbf{R}_p$  is the lateral regularisation matrix for the thicknesses and the velocities.
- $\mathbf{C}_{Rp}$  represent the covariance matrices.
- $\lambda$  is the Marquart damping parameter.
- $\mathbf{g}(\mathbf{m}_n)$  represent the forward response.

The entire set of 1D VS models  $\mathbf{m}$  is related to the entire local DC dataset  $\mathbf{d}_{obs}$  with the linked observational covariance matrix  $\mathbf{C}_{obs}$ . The efficacy of the  $\mathbf{R}_p$  matrix is function of the power of the constraints described in the covariance matrices. The non-linearity of the problem, particularly in the first iterations, is stabilised by  $\lambda$  while  $\mathbf{g}(\mathbf{m}_n)$  links the VS models to their relative SW dispersion curves. More details about the inversion algorithm can be found in Boiero, 2009.

### 6.3 APPLICATIO TO AURIGNAC DATA-SET

The method we adopted it is schematized in the flowchart in Figure 6.1

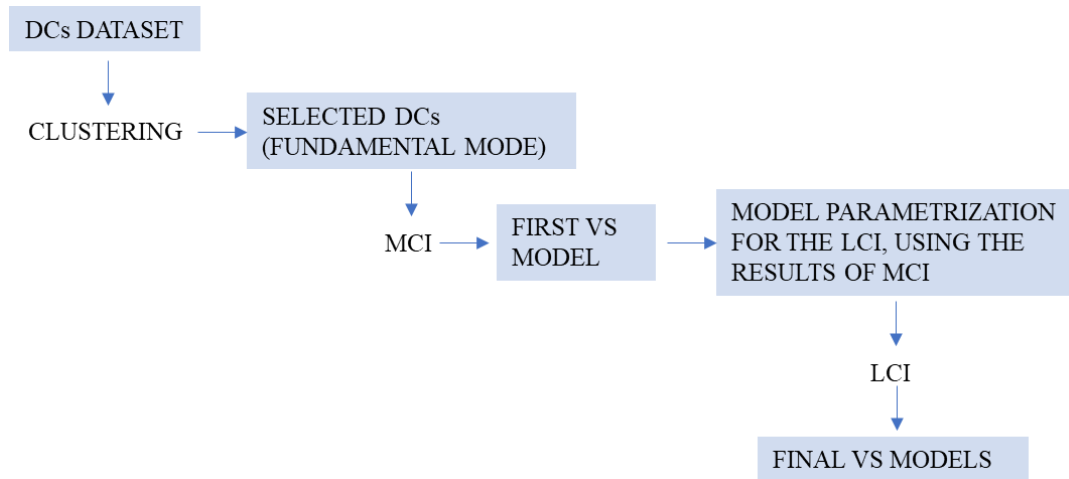


Figure 6.1-Flowchart LCI

The starting point of our method was the selection of the DCs (fundamental modes) to invert, to do so we clustered the data, as explained in the previous chapter. Once selected the DCs. We inverted them using the MCI to accomplish a rigorous model parameterization and, consequently we adopted the LCI of local DCs to get a final pseudo 3D model.

In the following will be presented all the results.

### 6.3.1 MCI RESULT

In Figure 6.2 a and b (from Khosro Anjom, 2021), we show the estimated VS (obtained through the MCI) for the two different clusters that we explained in section 4.3.

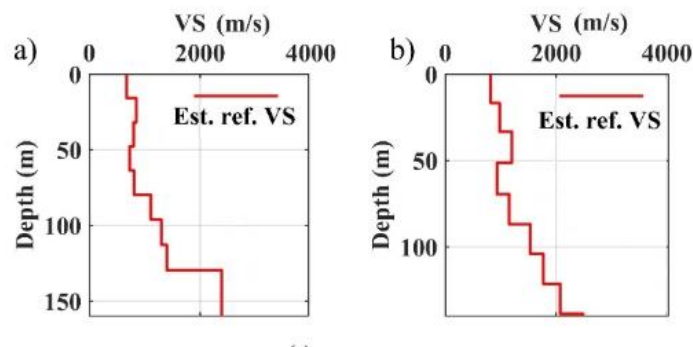


Figure 6.2-Estimated VS-(a) for the reference DC of Cluster A. (b) for the reference DC of Cluster B. (Khosro Anjom, 2021),

The selected model parameters for the LCI inversion are shown in Table 5.1:

Table 6.1-Model parameters

NUMBERS OF LAYER	DENSITY	POISSON RATIO
9 with a constant thickness of 15 meters, except for the first layer (20 m)	2400 Kg/m <sup>3</sup> in all the layers, excluded for the first one (2200 Kg/m <sup>3</sup> )	we use a priori Poisson's ratio from Khosro Anjom (2021). (Figure 5.2)

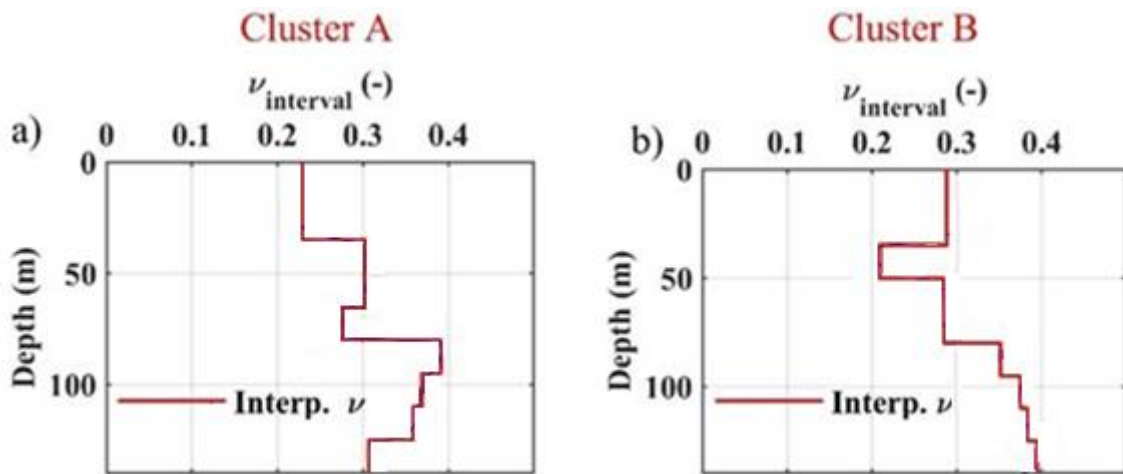


Figure 6.3-(a) The obtained Poisson's ratio for LCI application for cluster A. (b) The estimated Poisson's ratio for cluster B in blue. The obtained Poisson's ratio for LCI for cluster B.

### 6.3.2 LCI RESULT

For the LCI the level of constraints selected was 50 m/s, because Khosro Anjom (2021) demonstrated is the optimal level for this dataset.

The final output obtained selecting the laterally constrained inversion (50 m/s constraints) automatically ceased after 37 iterations, reaching a minimum misfit. In Figure 6.4a to d, we show the horizontal sections of the estimated VS model at various depths. In Figure 6.5(a) it is shown the quasi-3D view of the VS model, obtained after the interpolation of the estimate 1D models, and in Figure 6.5(b) we show multiple iso-surfaces in x, y, and z directions from the 3D model.

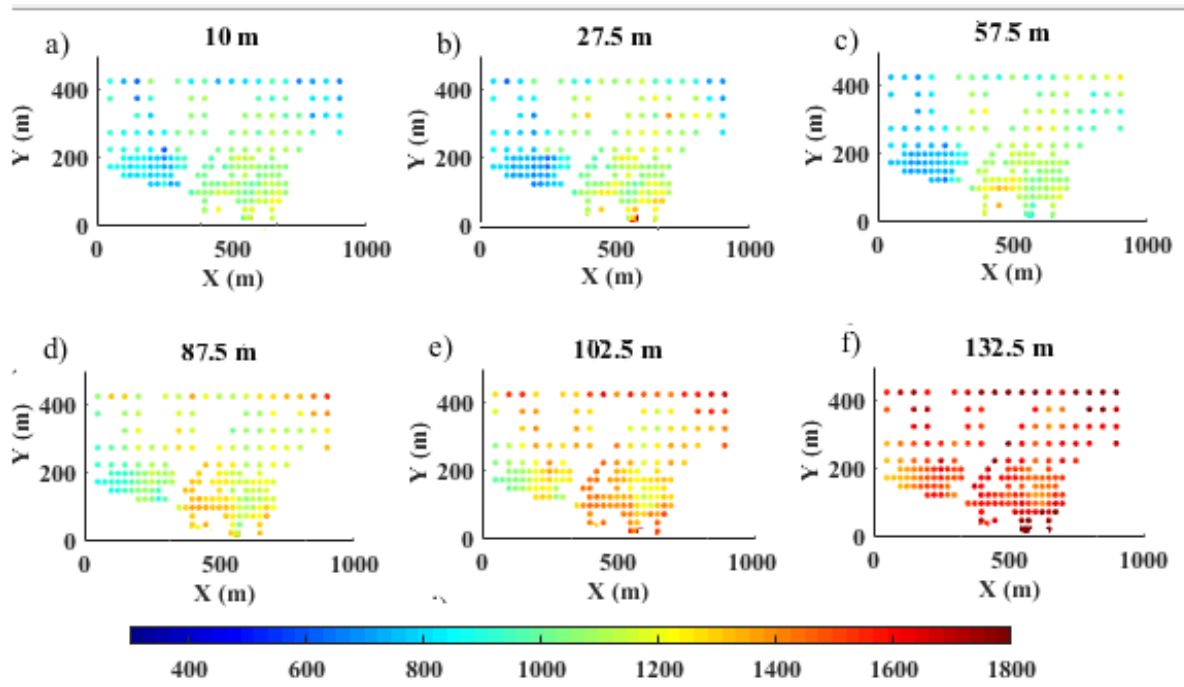


Figure 6.4--Horizontal sections of the estimated VS model at various depths

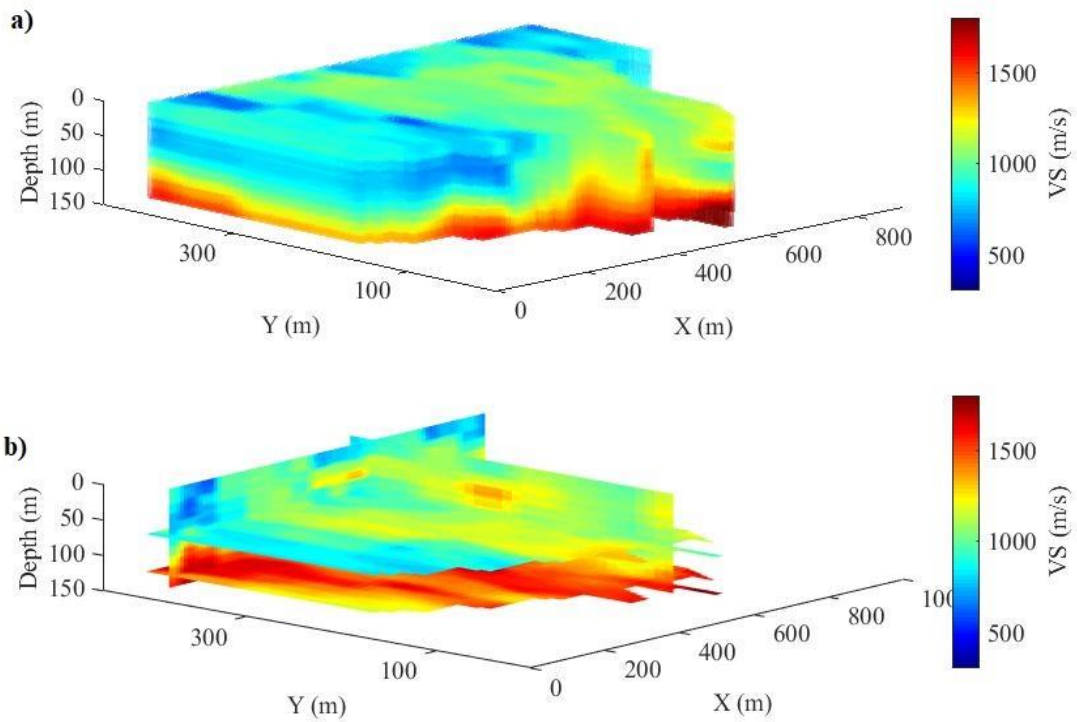


Figure 6.5- VS model- (a) 3D view of the obtained VS after linear interpolation of the 1D models. (b) Multiple iso-surfaces in x, y, and z directions from the 3D model.

## **6.4 CONCLUSION**

The tests conducted on the data acquired with the carpet acquisition show that the Laterally Constrained Inversion (LCI) is a powerful tool for consistent and reliable estimation of a VS model with lateral variations. both the processing and the constraints applied during the inversion produce a smoothing effect on the final VS model results.

## 7. MULTI-MODAL INVERSION

### 7.1 OVERVIEW

Generally, in surface wave analysis the VS model is obtained from the inversion of the fundamental modes of the observed DCs. However, it is reasonable to consider higher modes since, very often, the experimental DC is characterized by the superposition of numerous modes, especially in the case of velocity inversions or sharp velocity contrasts in the S-wave profile (Maraschini et al., 2010).

The main value of the higher modes is that they are sensitive to factors to which the fundamental mode is poorly sensitive (Socco and Strobbia, 2004). For these reasons, numerous authors analyze and underline the importance of higher modes in the inversion process.

Ernst, (2008), and Maraschini et al.,(2008) show that using them can enhance the correctness of the estimated velocity model, specifically in the occurrence of a low velocity layer (Gucunski and Woods, 1992; Xia et al., 2003). Gabriels et al., (1987) demonstrate higher modes can improve the investigation depth, Ernst, (2008), show that including them in the inversion can stabilize the process, in particular, in the case of not accessibility of the low-frequency band Xu et al., (2006), Xia et al. (2006) prove that they can improve the resolution of the shear wave velocity of the inverted model.

Those works validate the importance of higher modes in Rayleigh-wave inversion, but it is valuable to mention that including them in the inversion presents difficulties. For this reason, some authors analyze the common issues that derive from their use in the inversion process and present possible solutions.

One issue to consider is the separation of various modes in the spectrum. Gabriels et al. (1987) and Foti et al. (2000) underline that it is possible to improve spectral resolution while also saving high-frequency info, only by using many sensors and a long array. Park et al. (1999) and Luo et al. (2008) demonstrate that it is possible to enhance the mode separation during the signal-processing.

Another important issue to consider is the recognition of the mode number for every data point. This means that since part of the apparent DC could arise from the superposition of modes, some modes could be misidentified in the experimental data set. Therefore, if a portion of the DC is related to an improper mode number the resulting errors are greater than errors resulting from inaccurate data for a given mode (Zhang & Chan, 2003). Due to these considerations, few authors worked on multimodal inversions that do not require mode numbering.

Ganji et al. (1998), Lai & Rix (1999), Forbriger (2003a,b) make a comparison on the experimental apparent DC with a synthetic apparent DC or utilized the full waveform inversion. These methodologies are computationally costly since they need an accurate simulation of the wave propagation. Another method to invert higher modes, that does not require to number the different modes was proposed by Ernst (2007) and then implemented within a deterministic algorithm by Maraschini et al. (2010). This is the approach that we used for the inversion of the higher modes in this thesis. The inversion technique makes use of a misfit function based on the properties of the solution of the forward problem, allowing for a substantial saving of computational costs (Maraschini et al., 2010).

In the following section, after briefly explaining the approach introduced by Maraschini et al (2010), we apply it to the Aurignac dataset and subsequently we present the results.

## **7.2 MARASCHINI'S METHOD**

Maraschini and Foti (2010) developed a method to invert apparent DCs implementing in a Monte Carlo inversion the Haskell-Thomson matrix determinant misfit function. This permit to automatically consider all the modes preventing mode misidentification and with a reduced computational cost.

In particular, the method is based on a misfit function based on the determinant of the Haskell-Thomson matrix and a classical Euclidean distance between the dispersion curves.

Those misfits are utilized in a MCI with a large population of profiles. Consequently, the selection of representative models is achieved by using a Fisher test centred on the Euclidean distance between the experimental and the synthetic DCs to the best models of the MCI (Maraschini et al, 2010).

## **7.3 APPLICATION TO AURIGNAC DATASET**

In the following section we explain the criterion for the selection of the model space, and we show the result of the inversion.

### **7.3.1 MODEL SPACE**

The boundaries of the model space are VS and depth, while the Poisson ratio and the density are assumed, so they do not vary in the model space.

The boundaries are selected based on the result of the LCI. We decided to use the minimum and the maximum profiles of the VS to impose respectively the lower and the upper boundary limits of the models for the inversion of the higher modes. We did so, to obtain a result that could be in the range of the results of the LCI and to reduce the computational time.

We divided the analyzed area into two sub-areas (Chapter 4) using clustering, therefore we apply the same clustering also to define the model space based on the LCI inversion. We defined different model space boundaries for cluster A one for the cluster B: cluster A corresponds to the high-velocity area, while the cluster B corresponds to the low-velocity area. In Figure 7.1 we show the results of the LCI in terms of depth vs VS, for cluster A (in blue) and in Figure 7.2 for cluster B (in red).

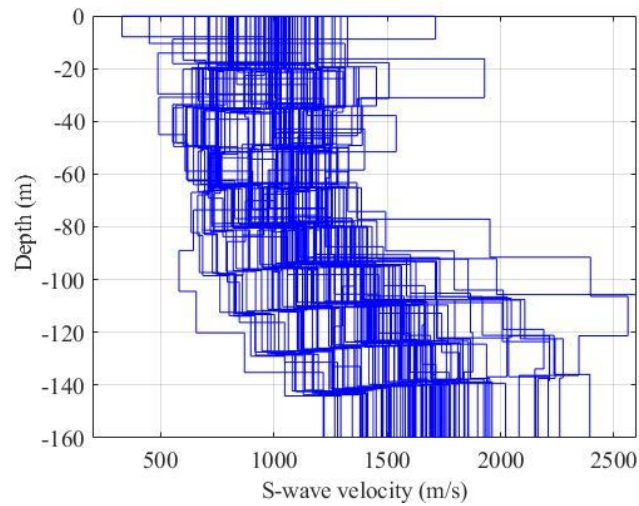


*Figure 7.1- LCI result for the high velocity area*

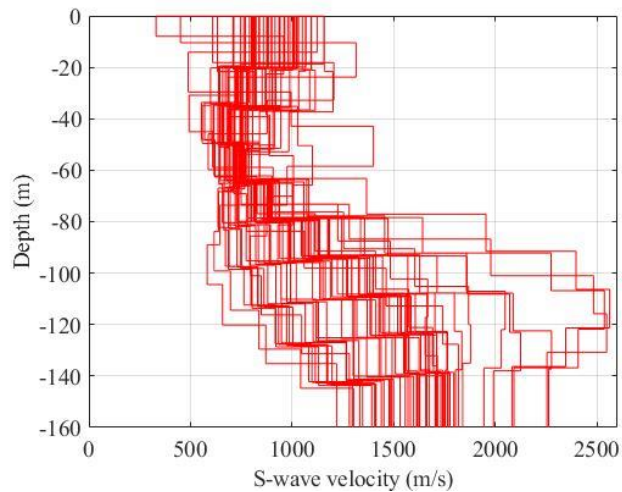


*Figure 7.2- LCI result for the low velocity area*

In both areas there is a general trend for many models and also some models that are far from the general trend, to be able to generate a proper model space, we removed these outliers, and reduced the reference models as those shown in Figure 7.3 and 7.4.

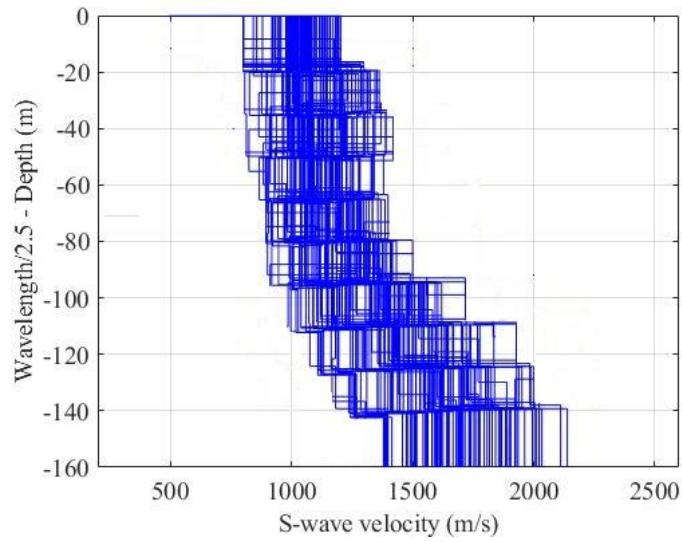


Figure 7.3-LCI result for the high velocity area after removing outliers

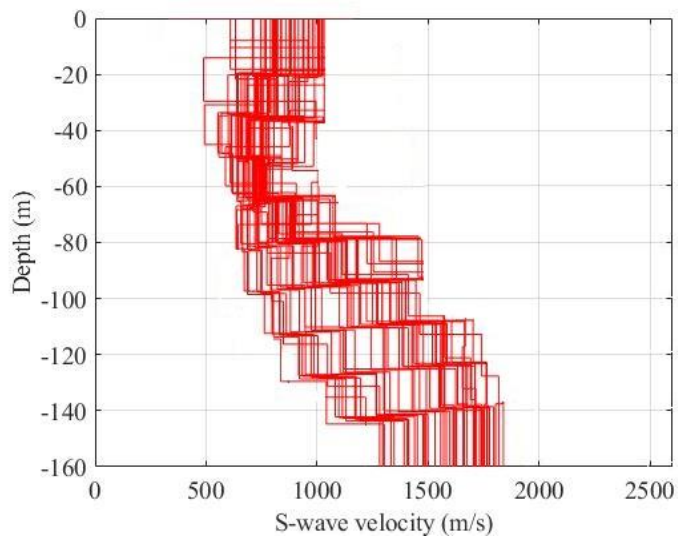


Figure 7.4LCI result for the slow velocity area after removing outliers

We then selected the boundaries of the model space for the inversion by defining the the minimum and the maximum profile of the VS vs depth. In Figures 7.5 and 7.6 we show the selected model space for the cluster A and B, respectively

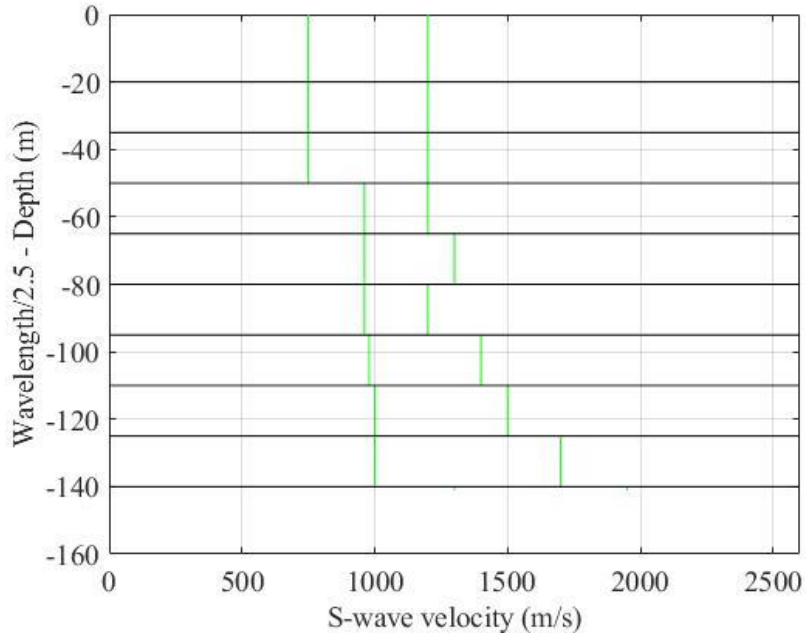


Figure 7.5-Final boundary for the high velocity area.

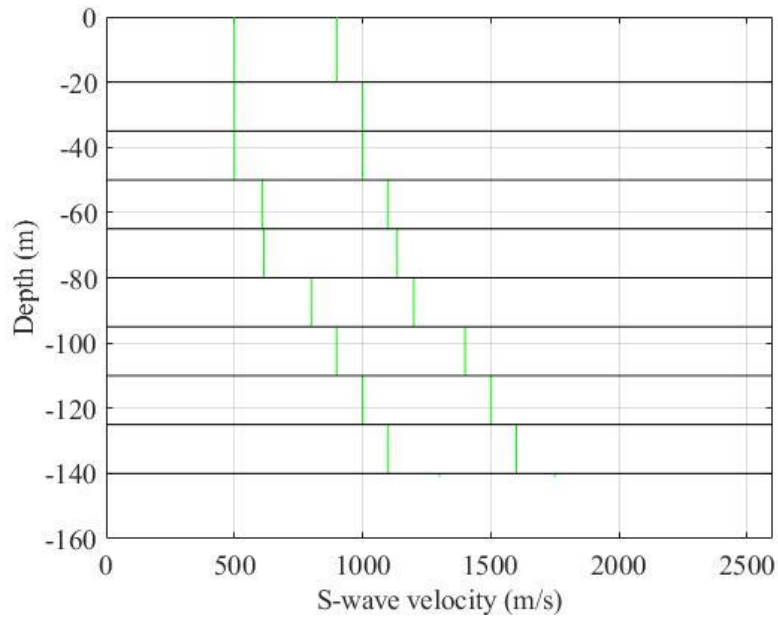


Figure 7.6-Final boundary for the low velocity area.

The MCI of the higher modes, for the parametrization of the model space we utilized the same parameters utilized in the LCI, so 9 layers with a constant thickness of 15 meters, except for the first layer (20 m), density equal to  $1800 \text{ Kg/m}^3$  and a priori Poisson's ratio from Khosro Anjom (2021). (Figure 5.2)

### 7.3.2 RESULTS

For the Monte Carlo inversion  $1 \times 10^6$  profiles were generated by random sampling VS within the boundaries.

For brevity we present the output only for one DC for each cluster.

For the cluster A, in Figure 7.7 it is shown the best plotted utilizing a color scale that is based on the fitting, the best fitting is characterized by the blue color, while for the lower misfit the yellow color is utilized. In Figures 7.8 and 7.9 we show the difference between the synthetic dispersion curve and the absolute value of the Haskell–Thomson matrix determinant of the best-fitting model, the fitting between the real dispersion curve and the dispersion curves of the best profiles.

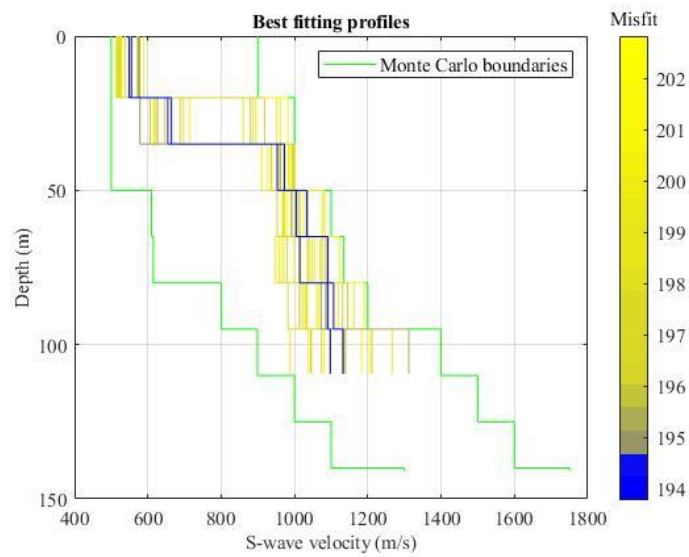


Figure 7.7-Best fitting profile for one sample of cluster A

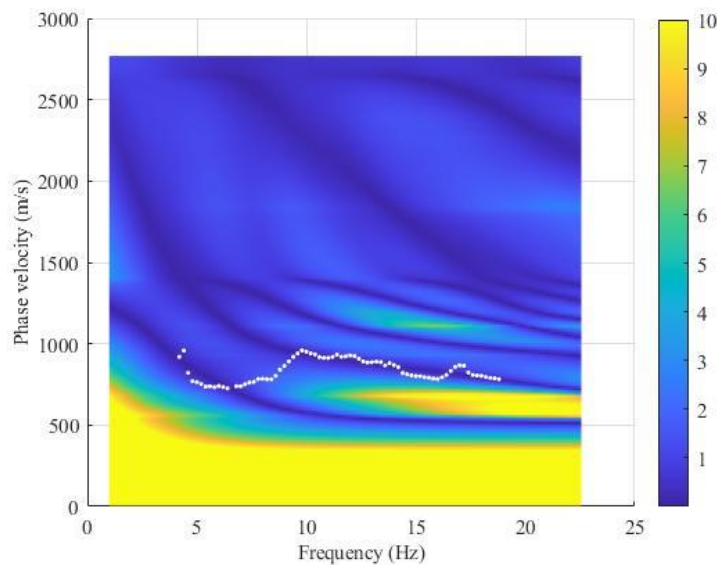


Figure 7.8-Absolute value of the Haskell–Thomson matrix determinant for best-fitting model of cluster A (white dots represent the experimental dispersion curve).

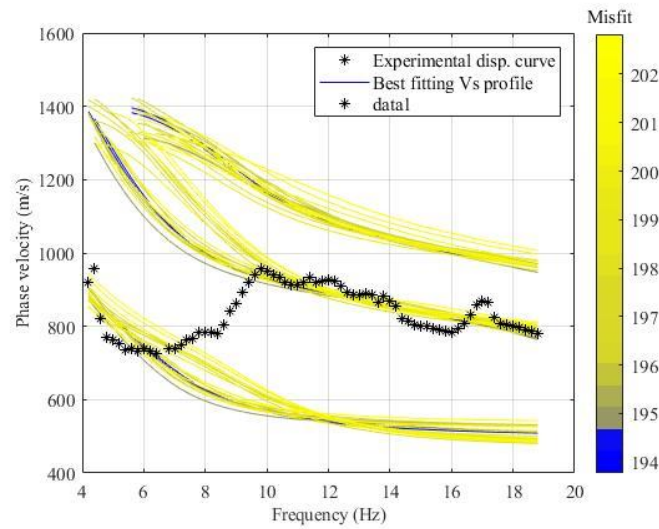


Figure 7.9-- Dispersion curves for best models compared with the experimental dispersion curve.

There is a good agreement among the real data and the synthetic DC. The experimental DC is characterized by the fundamental mode and the higher mode, but a few points do not fit to any mode, this is caused by the spatial resolution of the acquisition (Maraschini et al, 2010). They belong to the, so called, transition zones. The determinant misfit function, used in this work, permits to take into account the transition zones, indeed, the area in which the experimental DC jump from a mode to the next one is linked with low-misfit values (Figure 7.8).

For the cluster B, in Figure 7.10 we show the results using the same scheme adopted for cluster A.

In Figures 7.11 and 7.12 we show again the difference between the synthetic dispersion curve and the absolute value of the Haskell–Thomson matrix determinant of the best-fitting model, the fitting between the real dispersion curve and the dispersion curves of the best profiles.

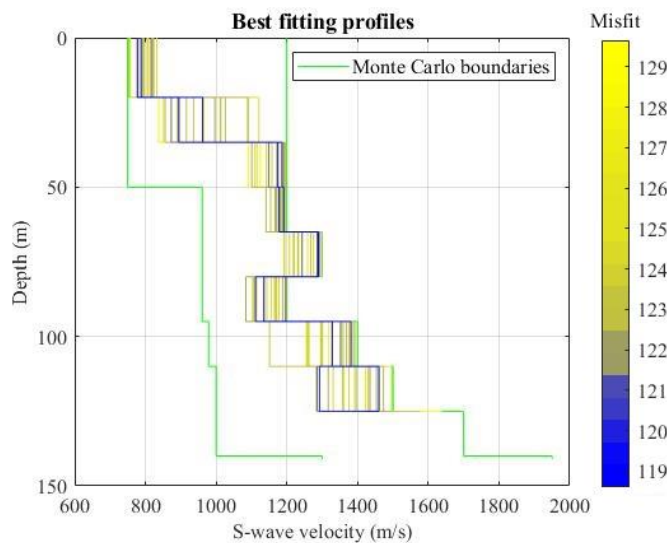


Figure 7.10-Best fitting profile for one sample of cluster B

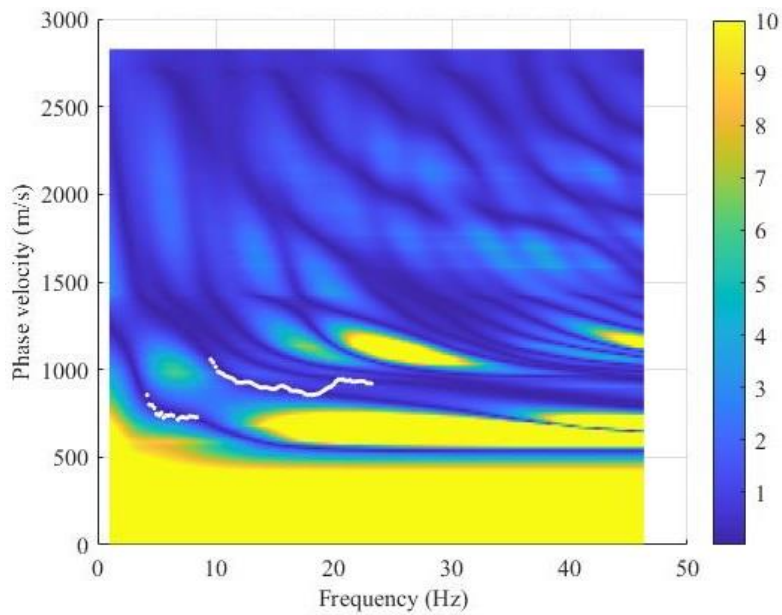


Figure 7.11- Absolute value of the Haskell–Thomson matrix determinant for best-fitting model of cluster B (white dots represent the experimental dispersion curve).

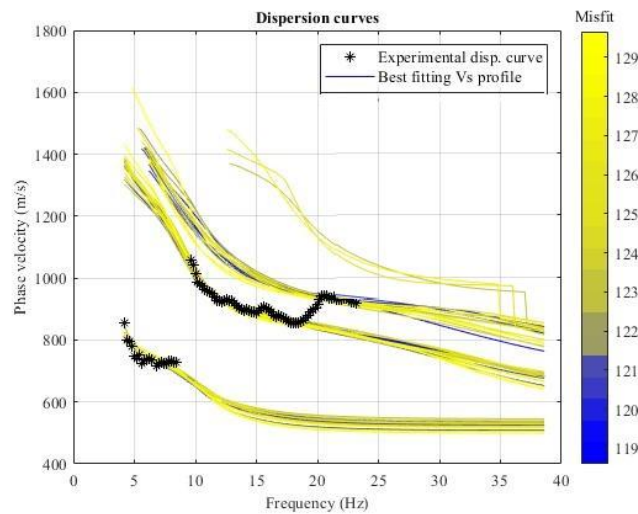


Figure 7.12- Dispersion curves for best models compared with the experimental dispersion curve.

We obtained a very good fitting between experimental and computed data. Also, in this case, there are some points in the transition zone.

To conclude, in Figure 7.13 we show the 3D view of the VS model, obtained after the interpolation of the estimate 1D models, and in Figure 7.13 (b) multiple iso-surfaces in x, y, and z directions from the 3D model

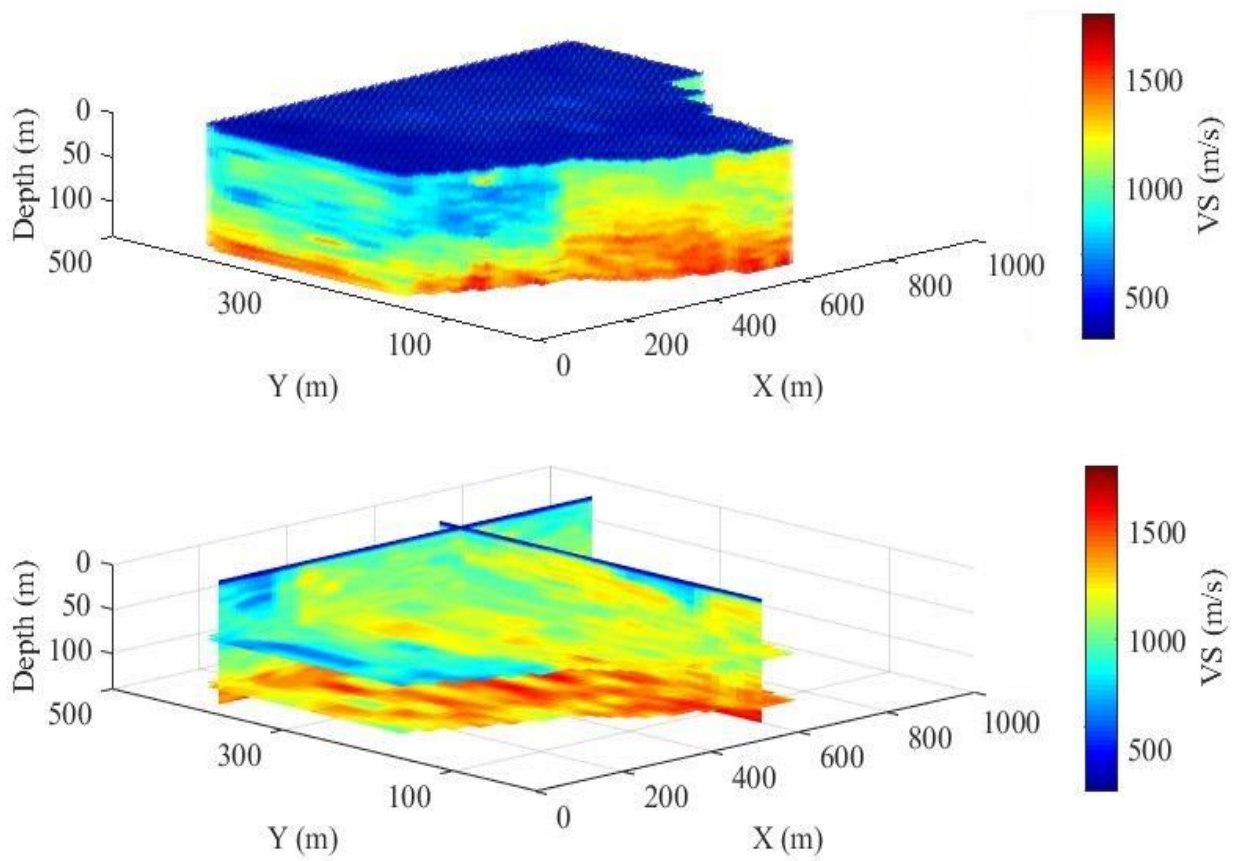


Figure 7.13-VS model (a) 3D view of the obtained VS after linear interpolation of the 1D models. (b) Multiple iso-surfaces in x, y, and z directions from the 3D model.

## 7.4 MULTIMODAL VS FUNDAMENTAL MODES INVERSION

Once obtained the results, we wanted to answer to an important question, does the inclusion of the higher modes in the Maraschini MCI, improve the quality of the obtained results?

To answer to this question we inverted, for some DCs, the fundamental mode only using the same algorithm used for the multimodal inversion and we compared the results with those obtained by including higher mode data points.

In Figure 7.14 it is shown the comparison of the inversion. In Figure 7.14 (a) we show the result of the inversion considering the fundamental mode only and in Figure 7.14 (b) the result of the inversion also considering the higher modes.

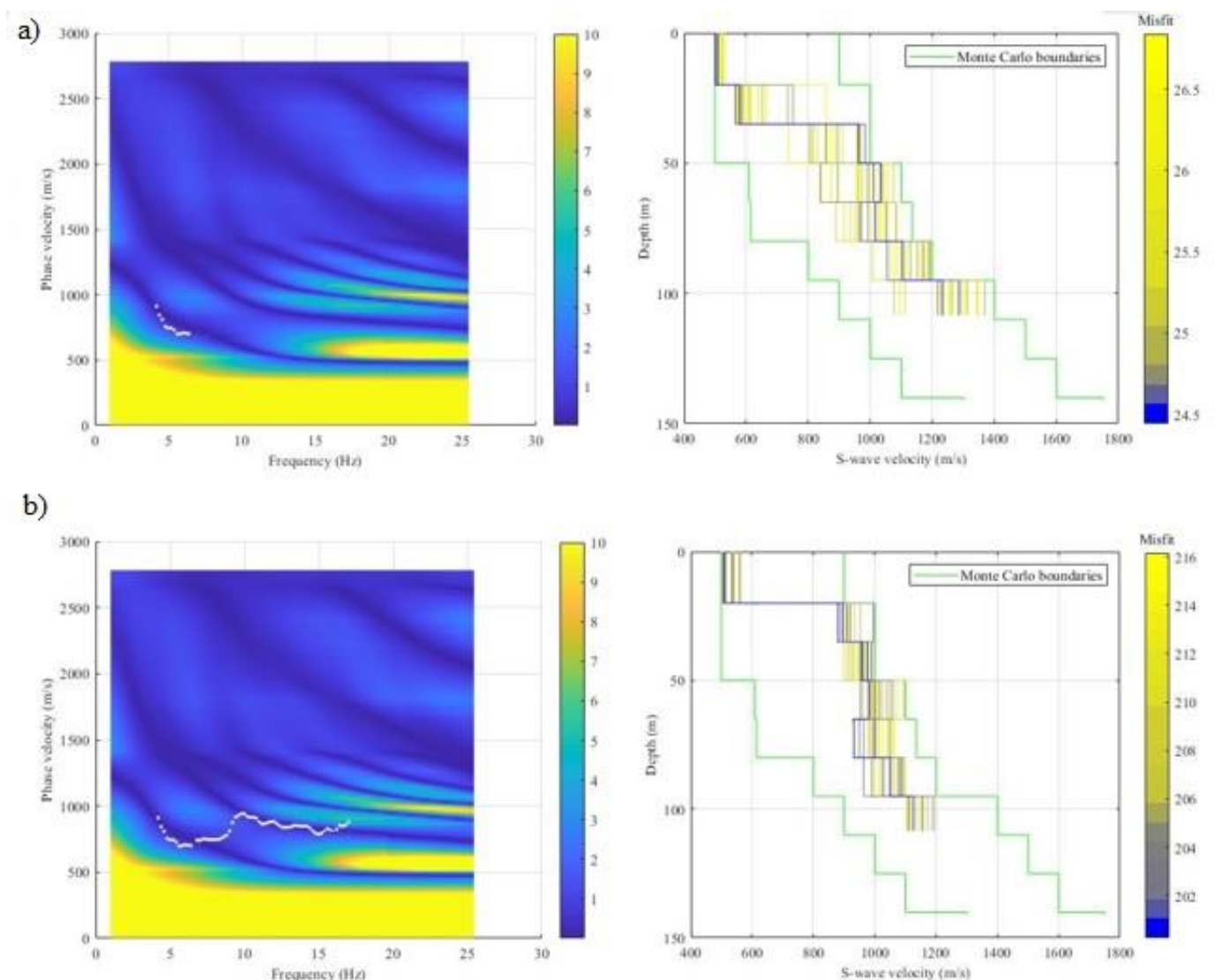


Figure 7.14-Comparison of the inversions (a) result of the inversion considering only the fundamental mode, (b) the result of the inversion also considering the higher modes.

As it is possible to notice, in Figure 7.14(d) the obtained profiles present a lower variation in comparison with the profile of Figure 7.14(b). This means that including the higher modes in the inversion, increase the resolution of the process.

## **7.5 CONCLUSION**

In this chapter, we proposed the Maraschini-Monte Carlo algorithm for surface wave inversion (higher modes) based on a determinant misfit function. This misfit presents two central benefits. The main one is that it allows all the experimental higher modes to be considered in the inversion, without the need to number the modes before the inversion. The second advantage is that the computation of the misfit is faster than the usual misfit functions. For the inversion of the multimodal generating 1 million model the computational time was equal to 10 minutes for each DCs.

The efficacy of this process is demonstrated by the results obtained from the application on the Aurignac dataset, where the algorithm is assessed by inverting DCs that present complexities, for example the jump of the apparent DC to higher modes.

Moreover, we showed the importance of including the higher modes during the inversion, indeed, as it is demonstrated by the results obtained, higher modes increase the resolution at depth in comparison with the inversion of the fundamental mode only.

## 8. COMPARISON OF THE METHODS

### 8.1 INTRODUCTION

The goal of this chapter is to compare the results obtained from the fundamental modes inversion LCI, and the results from the Multi-modal Monte Carlo inversion, we compared the relative results to evaluate the strength and the weakness of the utilized approaches, moreover, our task is also to underline advantages obtained from the inversion of the higher modes. We divide this chapter into two parts, first we present a graphical analysis, in which we show the chart of the local estimated VS model at various depths for both analyses, then we present a quantitative analysis to better understand the magnitude of the similarity or dissimilarity of the two different inversions.

### 8.2 GRAPHICAL ANALYSIS

We present the obtained results in terms of shear wave velocity at various depths: 20 meters, 50 meters, 80 meters, 100 meters, and 130 meters.

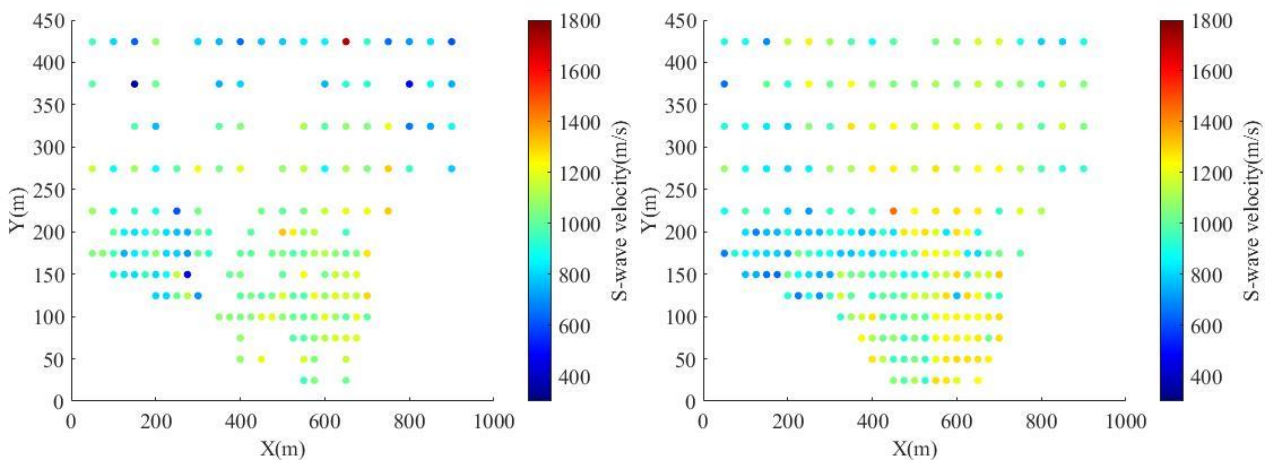


Figure 8.1- The estimated VS model at a depth equal to 20 meters, (a) results from LCI, (b) results from multi-modal Monte Carlo Inversion

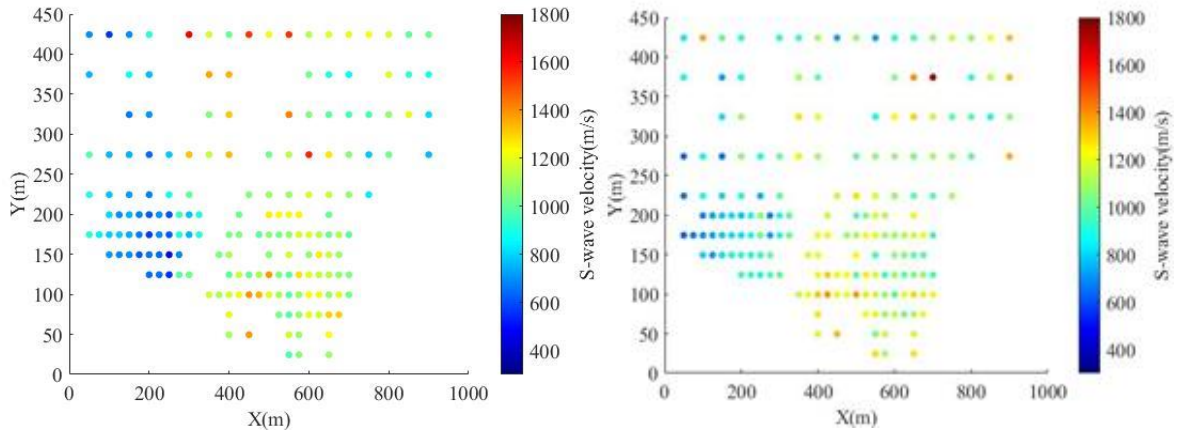


Figure 8.2-The estimated VS model at a depth equal to 50 meters, (a) results from LCI, (b) results from multi-modal Monte Carlo Inversion

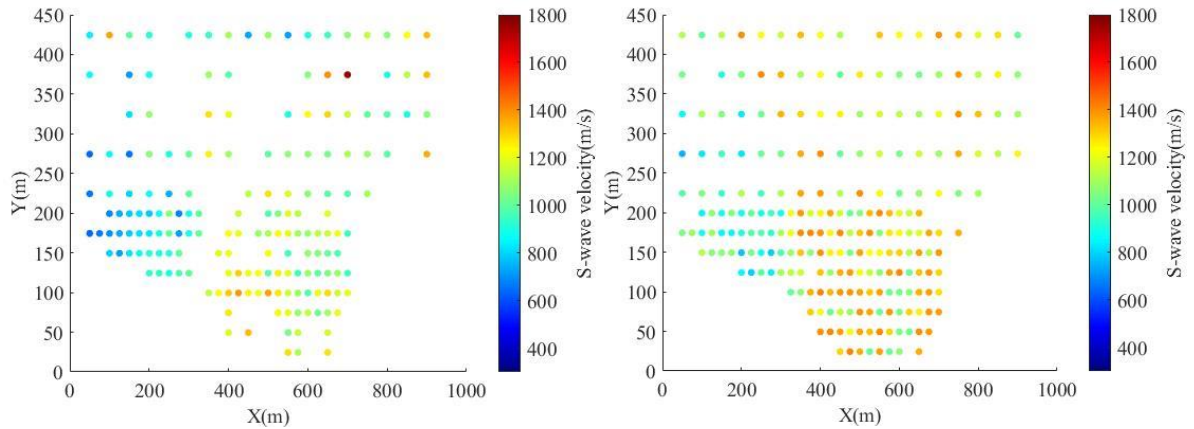


Figure 8.3-The estimated VS model at a depth equal to 80 meters, (a) results from LCI, (b) results from multi-modal Monte Carlo Inversion

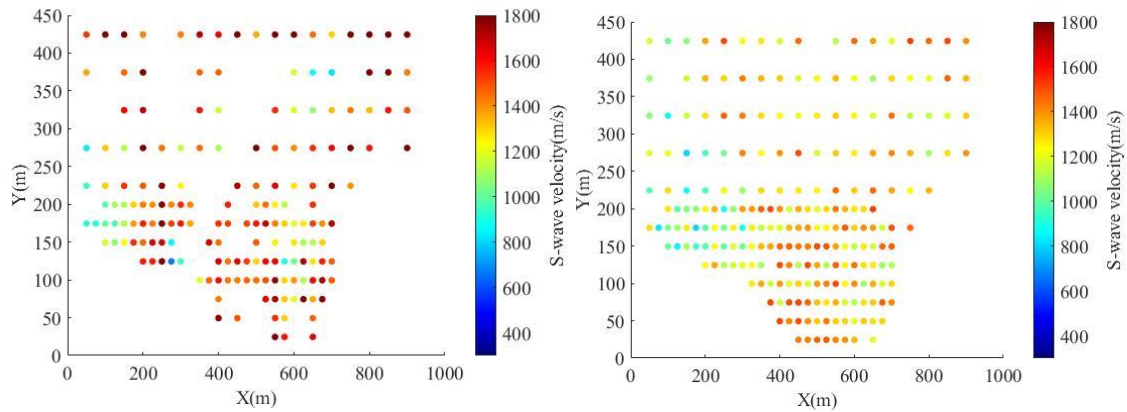


Figure 8.4-The estimated VS model at a depth equal to 100 meters, (a) results from LCI, (b) results from multi-modal Monte Carlo Inversion

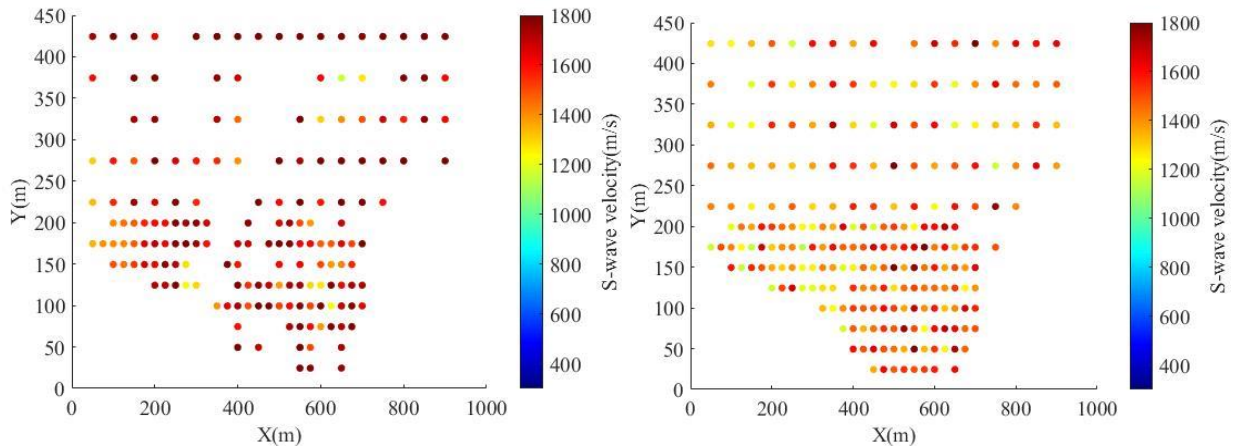


Figure 8.5-The estimated VS model the at a depth equal to 130 meters, (a) results from LCI, (b) results from multi-modal Monte Carlo Inversion

As it is possible to notice from the above figures, globally the results obtained from the two different inversions are comparable. Both models show velocity contrast between the east and west sides of the site.

In particular, it is possible to notice that until the depth of 80 meters the VS are almost the same with just a few points in which the result differs more, once reached the depth of 100 meters the difference between the two results increases.

In the case of multimodal inversion, we obtained more models, as a consequence the best techniques in terms of amount of results it the multimodal inversion.

### 8.3 QUANTITATIVE ANALYSIS

In this section, we evaluate the difference between the VS obtained for the two different inversions, in table 5 we show for each selected depth:

- the average VS variation,
- the minimum VS variation
- the maximum VS variation

And in table 6, we show for each selected depth, the percentage of:

- the average VS variation,
- the minimum VS variation,
- the maximum VS variation,

Computed with the following equations:

$$\text{Average VS variation } \left[ \frac{m}{s} \right] = \text{mean}(VS_{LCI_i} - VS_{MCI_i})$$

$$\text{Average VS variation } [\%] = \text{mean} \left( \left| \frac{VS_{LCI_i} - VS_{MCI_i}}{VS_{LCI_i}} \right| \times 100 \right)$$

Where:

- $VS_{LCI_i}$  represent the value of the shear wave velocity from the LCI, at a given depth,
- $VS_{MCI_i}$  represent the value of the shear wave velocity from the LCI, at a given depth

*Table 8.1-Variation of the VS result of the higher modes in comparison with the result of the fundamental modes*

SELECTED DEPTH [m]	AVERAGE VARIATION [m/s]	MINIMUM VARIATION [m/s]	MAXIMUM VARIATION [m/s]
20	131	1	379
50	116	2	462
80	111	0,2	515
100	216	0,8	1184
130	209	4	1202

Table 8.2-Variation in percentage of the VS result of the higher modes in comparison with the result of the fundamental modes

SELECTED DEPTH [m]	AVERAGE VARIATION [%]	MINIMUM VARIATION [%]	MAXIMUM VARIATION [%]
20	10	0,10	105
50	10	0,24	72
80	9	0,01	50
100	11	0,05	61
130	11,5	0,23	41

The differences between the two models are within 10%, the most comparable results are obtained at the depth of 80 meters, in which the average variation it is only 9 percent, while the worst condition it is at the depth of 130 meters where the average variation is equal to 11,5 percent. In the following figure, we show the results in terms of variation in VS both in terms of [m/s] and [%],

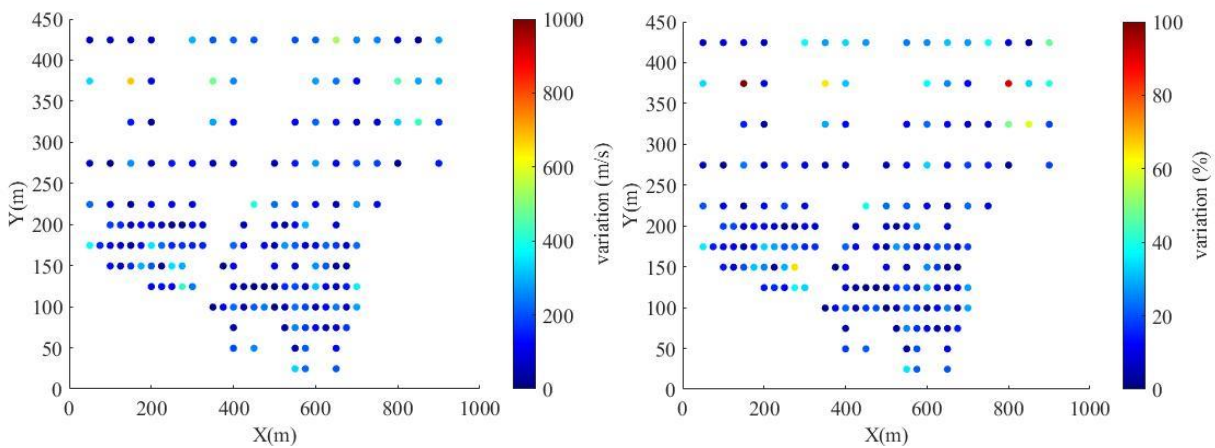


Figure 8.6-Variation of VS model at a depth equal to 20 meters, (a) variation in terms of (m/s), (b) variation in terms of (%)

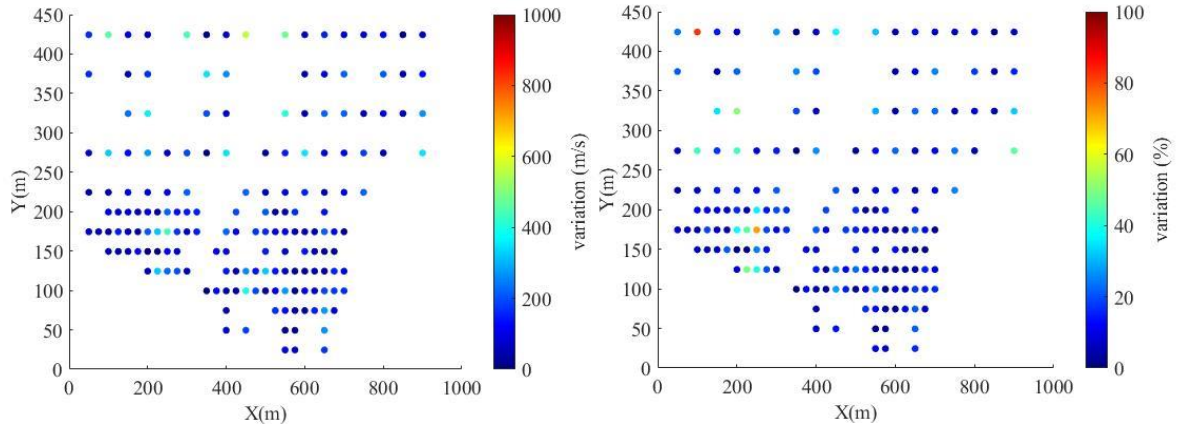


Figure 8.7-Variation of VS model at a depth equal to 50 meters, (a) variation in terms of (m/s), (b) variation in terms of (%)

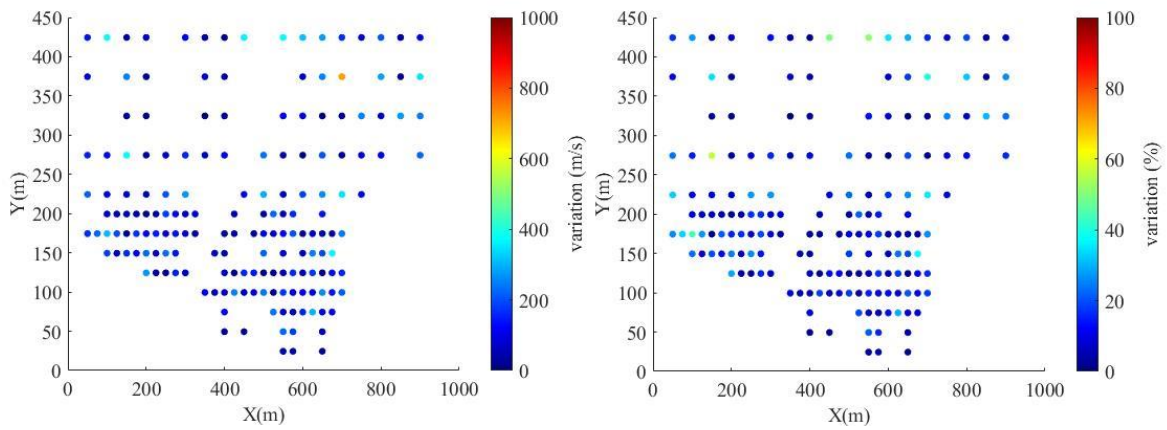


Figure 8.8-Variation of VS model at a depth equal to 80 meters, (a) variation in terms of (m/s), (b) variation in terms of (%)

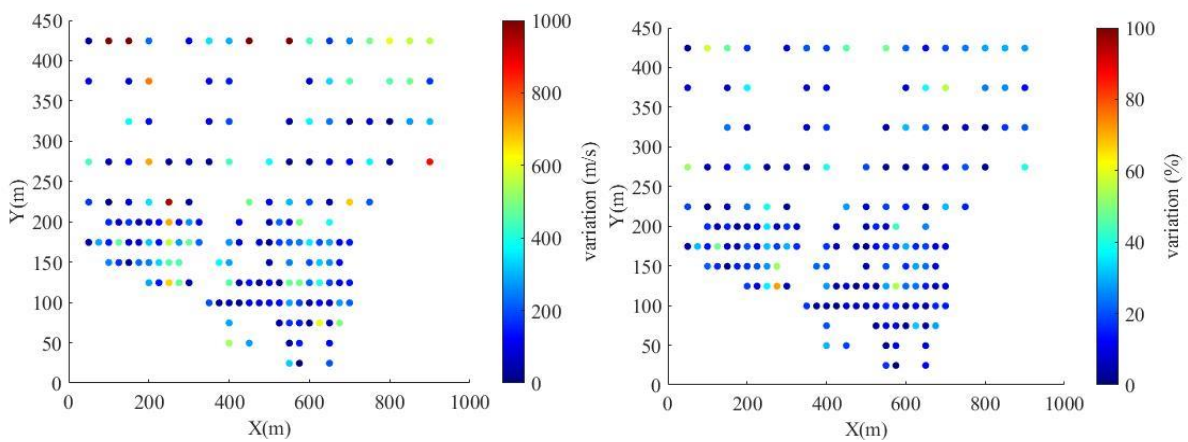


Figure 8.9-Variation of VS model at a depth equal to 20 meters, (a) variation in terms of (m/s), (b) variation in terms of (%)

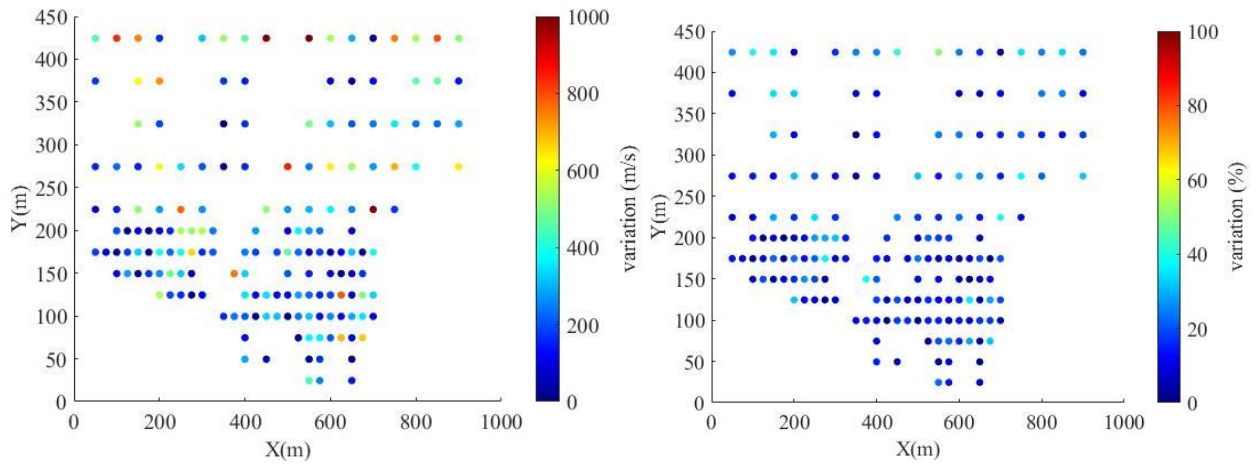


Figure 8.10-Variation of VS model at a depth equal to 130 meters, (a) variation in terms of (m/s), (b) variation in terms of (%)

The higher amount of variation is located in the north part of the investigated area, that corresponds also to the area in which there is a lower density of receivers, on the other hand, in the south part of the area (the high-density receiver zone), the variation is less.

## CONCLUSION

In this thesis, we presented a case study that confirms the feasibility and validity of the new non-standard scheme of acquisition, carpet receiver geometry and irregular sparse sources, merged with a fast-processing technique, a so-called square multichannel, for the extraction of the DCs

We considered a dataset, acquired in a mining site in the province of Aurignac, south France, characterized by stiff materials, consisting of seismic gathers recorded using an array of 217 5 Hz geophones, deployed using the carpet acquisition scheme.

In the first part of the thesis, we implemented a processing workflow based on a square moving window that span the whole area and identifies a set of receivers which are used to estimate a dispersion curve using the phase shift data transform on which the maxima are automatically picked. For each position of the moving window we considered separately all the shots identified by a circular area centered in the square center. The velocity spectra from the different shots were stacked to improve the quality of the DCs. . We considered the obtained dispersion curves as a local property of the subsurface and associated them to the coordinates of the center of the window and the data that we inverted was composed by a group of DCs. As is usual, in the case of stiff sites, the data were noisy, discontinuous, narrow banded and characterized by the presence of energetic higher modes of propagation. We retrieved 173 dispersion curves for the inversion of the fundamental's modes and 234 for the inversion of the higher modes.

We first inverted the fundamental curves using a laterally constrained inversion (LCI). The obtained results demonstrated that the LCI is a powerful tool for consistent and reliable estimation of a VS model with lateral variations.

Due to the large amount of information that is contained in the higher modes we also included them in the inversion. We applied the Maraschini-Montecarlo algorithm for the multi-modal inversion. The results showed the efficacy of the used algorithm in inverting DCs that present complexities, for example, the jump of the apparent DC to higher modes.

Furthermore, we demonstrated by comparing the results obtained from the Monte Carlo multi-modal inversion with the Monte Carlo inversion of the individual fundamental mode, that including the higher modes improves the quality of the results. In our case, the use of the higher modes increased the resolution of the velocity model at depth.

We compared the results obtained from the two analyses (LCI and Monte Carlo multi-modal) in terms of variation of shear wave velocity, the retrieved VS values achieved are, globally, comparable with an average variation of 10%.

The obtained outcomes have shown that our method properly worked on the data acquired with the new acquisition approach. Pondering all these features, we conclude that the new acquisition scheme system merged with a fast processing approach, is functional to build shear wave velocity models in an area characterized by stiff materials.

## REFERENCES

- Aki K., and P. G. Richards, 2002, Quantitative seismology. Theory and methods: W.H. Freeman and Company.
- Auken, E., and A. V. Christiansen, 2004, Layered and laterally constrained 2D inversion of resistivity data: *Geophysics*, 69, 752–761.
- Auken, E., A. V. Christiansen, B. H. Jacobsen, N. Foged, and K. I. Sørensen, 2005, Piecewise 1D laterally constrained inversion of resistivity data: *Geophysical Prospecting*, 53, 497–506.
- Blacquiere G., and S. Nakayama, 2019, Optimum seismic acquisition geometry design with the help of artificial intelligence: *SEG Technical Program Expanded Abstracts*, 117-121
- Banab K., and D. Motazedian, 2010, On the Efficiency of the Multi-Channel Analysis of Surface Wave Method for Shallow and Semi-Deep Loose Soil Layers. *International Journal of Geophysics*, 55/2010/403016.
- Bardainne T., Garceran K., Retailleau M., Duwattez X., Sternfels R., & le meur David., 2017, Laterally Constrained Surface Wave Inversion. 10.3997/2214-4609.201700958.
- Bergamo P., Comina C., Foti ., Maraschini M., 2011, Seismic characterization of shallow bedrock sites with multimodal Monte Carlo inversion of surface wave data. *Soil Dynamics and Earthquake Engineering*. 31. 530–534.
- Boiero D., and L. V. Socco, 2011, The meaning of surface wave dispersion curves in weakly laterally varying structures: *Near Surface Geophysics*, 9, 561–570.
- Boiero D., 2009, Surface wave analysis for building shear wave velocity models, PhD thesis, Politecnico di Torino, Torino, Italia.
- Curtis A., and A. Lomax, 2001, Prior information, sampling distributions, and the curse of dimensionality: *Geophysics*, 66, 372-378.
- Ernst F., 2007, Long-wavelength statics estimation from guided waves, in *Proceedings of the 69th EAGE Conference and Exhibition, Extended Abstracts*, E033, London, UK.
- Ernst F., 2008. Multi-mode inversion for  $V_p$  and thick near-surface layers, in *Proceedings of the Near Surface 2008 14th European Meeting of Environmental and Engineering Geophysics*, Krakow, Poland.
- Forbriger, T., 2003a. Inversion of shallow-seismic wavefields. Part I. Wavefield transformation, *Geophys. J. Int.*, 153(3), 719–734.
- Forbriger, T., 2003b. Inversion of shallow-seismic wavefields. Part II. Inferring subsurface properties from wavefield transformation, *Geophys. J. Int.*, 153(3), 735–752.
- Foti S., L. Sambuelli, L. V. Socco, and C. Strobbia, 2003, Experiment of joint acquisition of seismic refraction and surface wave data, *Near Surface Geophysics* 1, 119–129.
- Foti S., Hollender F., Garofalo F. *et al.*, 2018, Guidelines for the good practice of surface wave analysis: a product of the InterPACIFIC project. *Bull Earthquake Eng* **16**, 2367–2420.

- Gucunski N. and R. D. Woods, 1991, Inversion of Rayleigh wave dispersion curve for SASW test, Proceedings of the 5th Conference on Soil Dynamics and Earthquake Engineering, Karlsruhe, pp. 127–138.
- Gabriels P., R. Snieder, and G. Nolet, 1987, In situ measurement of shearwave velocity in sediments with higher-mode Rayleigh waves, *Geophysical Prospecting* 35, 187–196.
- Ganji V., Gucunski, N., Nazarian, S., 1998. Automated inversion procedure for spectral analysis of surface waves, *J. Geotech. Geoenviron. Eng.*, 124(8), 757–770.
- Grandjean G., and A. Bitri, 2006, 2M-SASW: Multifold multichannel seismic inversion of local dispersion of Rayleigh waves in laterally heterogeneous subsurfaces: Application to the Super-Sauze earthflow, France: *Near Surface Geophysics*, 4, 367–375.
- Gucunski, N. and Woods, R.D., 1992. Numerical simulation of the SASW test, *Soil Dyn. Earthq. Eng.*, 11(4), 213–228.
- Hashemi Jokar, M., Boaga, J., Petronio, L., et al. 2019, Detection of lateral discontinuities via surface waves analysis: a case study at a derelict industrial site, *Journal of Applied Geophysics*, pp. 65-74.
- Hashemi M., H. Rahnema, A. Baghlani, 2020. Dispersion curves for media with lateral variation at different angles. *Scientia Iranica*. 10.24200/sci.2021.53575.3313.
- Hayashi, K. and Suzuki, H., 2004, CMP cross-correlation analysis of multi-channel surface-wave data, *Exploration Geophysics*, 35 (1), pp. 7-13.
- Khosro Anjom. F., F. Arabi, L. V. Socco, and C. Comina, 2018. Application of a method to determine S and P wave velocities from surface waves data analysis in presence of sharp lateral variations, in 36th GNGTS national convention, Expanded Abstracts.
- Khosro Anjom. F., 2021 (submitted), S-wave and P-wave velocity model estimation from surface waves, Ph.d. Thesis, Politecnico di Torino.
- Lai, C.G., Rix, G.J., 1999. Inversion of multi-mode effective dispersion curves, in *Pre-Failure Deformation Characteristics of Geomaterials*, pp. 411–418.
- Luke B., C. Calderón, R. C. Stone, and M. Huynh, 2003, Nonuniqueness in inversion of seismic surface-wave data: Proceedings of Symposium on the Application of Geophysics to Engineering and Environmental Problems (SAGEEP), Environmental and Engineering Geophysical Society, Denver.
- Luo, Y., Xia, J., Liu, J., et al., 2008, Generation of a pseudo-2D shear-wave velocity section by inversion of a series of 1D dispersion curves, *Journal of Applied Geophysics*, 64 (3-4), pp. 115-124 .
- Lys P. O., K. Elder, and J. Archer, 2018, "METIS, A Disruptive R&D Project To Revolutionize Land Seismic Acquisition." Paper presented at the SEG/AAPG/EAGE/SPE Research and Development Petroleum Conference and Exhibition, Abu Dhabi, UAE.
- Masoni I., B. Pagliccia, G. Thalmann, 2019 "The Use of Drones for Innovative Seismic Acquisition: A Change of Paradigm for HSE." Paper presented at the International Petroleum Technology Conference, Beijing, China.
- Miller R. D., J. Xia, C. B. Park, J. C. Davis, W. T. Shefchik, and L. Moore, 1999, Seismic techniques to delineate dissolution features in the upper 1000 ft at a power plant site, *SEG Technical Program Expanded Abstracts*, 492-495.

- Maraschini M., 2008, A new approach for the inversion of Rayleigh and Scholte waves in site characterization: Ph.D. dissertation, Politecnico di Torino.
- Maraschini M., F. Ernst, D. Boiero, S. Foti, and L. V. Socco, 2008, A new approach for multimodal inversion of Rayleigh and Scholte waves: 70th Conference and Technical Exhibition, EAGE, Extended Abstracts, D036.
- Maraschini M., F. Ernst, S. Foti, and L. V. Socco, 2010, A new misfit function for multimodal inversion of surface waves: *Geophysics*, 75, no. 4.
- Maraschini M., and S. Foti, 2010, A Monte Carlo multimodal inversion of surface waves: *Geophysical Journal International*, 182, no. 3, 1557–1566.
- Menke W. 1989. *Geophysical Data Analysis: Discrete Inverse Theory*. International Geophysics Series. San Diego: Academic Press.
- Maimon O., and L. Rokach. 2010. *Data Mining and Knowledge Discovery Handbook* (2nd ed.). Springer Publishing Company, Incorporated. doi: 10.1007/978-0-387-09823-4
- Neducza B., 2007, Stacking of surface waves: *Geophysics*, 72, no. 2, V51– V58.
- Okada H., 2003, The microtremor survey method: Geophysical monograph series 12, SEG, Tulsa, USA.
- Pan E., Chen X, Wang J, Yang Z, Zhang D, 2019, Sensitivity analysis of dispersion curves of Rayleigh waves with fundamental and higher modes, *Geophysical Journal International*, Volume 216, Issue 2, Pages 1276–1303,
- Park C., R. D. Miller, and J. Xia, 1998, Imaging dispersion-curves of surface waves on multichannel records: 68th Annual International Meeting, SEG, Expanded Abstracts, 1377–1380.
- Park C.B., R.D. Miller and J. Xia, 1999. Multichannel analysis of surface waves. *Geophysics* 64, 800–808.
- Park C.B., R.D. Miller and J. Xia, 2001, Offset and resolution of dispersion curve in multichannel analysis of surface waves (MASW): Proceedings of the SAGEEP 2001, Denver, Colorado, SSM-4.
- Park C. B., and M. Carnevale, 2010, Optimum MASW Survey--Revisit after a Decade of Use, *GeoFlorida: Advances in Analysis, Modeling and Design* . GSP 199.
- Puntous H., F. Adler, C. Strobbia, E. Masini, and S. Calassou, 2018 Revisiting Pyrenean foothills structural imaging by seismic interpretation in the shot domain: case study from 2D ECORS, Aquitaine Basin, France. 80 th EAGE Conference and Exhibition, Extended Abstracts, submitted.
- Rassenfoss S., 2017, This Vision of Onshore Seismic May Look Strange at First: *Journal of Petroleum Technology*, 34-38.
- Richart F.E. Jr., R.D. Woods, and J.R. Hall, 1970, *Vibration of soil and foundations*, Prentice-Hall, New Jersey.
- Sambridge M., and K. Mosegaard, 2002, Monte Carlo Methods in Geophysical Inverse Problems: *Rev. Geophys.*, 40, no. 3, 1-29.
- Socco L.V. and Strobbia, C., 2004. Surface-wave method for near surface characterization: a tutorial, *Near Surface Geophys.*, 2(4), 165–185.

- Socco L. V., and D. Boiero, 2008, Improved Monte Carlo inversion of surface wave data: *Geophysical Prospecting*, 56, 357- 371.
- Socco L.V., D. Boiero, C. Comina, S. Foti, and R. Wisén, 2008, Seismic characterisation of an alpine site: *Near Surface Geophysics*, 6, 253-265.
- Socco L.V., Boiero, D., Foti, S. and Wisen, R., 2009. Laterally constrained inversion of ground roll from seismic reflection records, *Geophysics*, 74(6), G35–G45.
- Socco L.V., Foti, S. and Boiero, D., 2010. Surface-wave analysis for building near-surface velocity models—established approaches and new perspectives, *Geophysics*, 75(5), A83–A102.
- Song Y.Y., J. P. Castagna, R. A. Black, and R. W. Knapp, 1989, Sensitivity of near-surface shear-wave velocity determination from rayleigh and love waves, *SEG Technical Program Expanded Abstracts*, 509-512.
- Tarantola A., 2005, *Inverse problem theory and methods for model parameter estimation*. Siam, Philadelphia, 1-55.
- Tian, G., Steeples, D.W., Xia, J., et al., 2003, Useful resorting in surface-wave method with the autojuggie", *Geophysics*, 68 (6), pp. 1906-1908.
- Wang L., J. Xia, Y. Xu, and Y. Luo, 2015, Numerical investigation of 3D MASW technique. 269-272. 10.1190/nsapc2015-071.
- Wang L., Luo, Y., Xu, Y., 2012. Numerical investigation of Rayleigh wave propagation on topography surface. *J. Appl. Geophys.* 86, 88–98.
- Wisén, R., and A. V. Christiansen, 2005, Laterally and mutually constrained inversion of surface wave seismic data and resistivity data: *Journal of Environmental & Engineering Geophysics*, 10, 251–262.
- Wisén, R., E. Auken, and T. Daklin, 2005, Combination of 1D laterally constrained inversion and 2D smooth inversion of resistivity data with a priori data from boreholes: *Near Surface Geophysics*, 3, 71–79.
- Xia J., Miller R.D. and Park C.B. 1999. Estimation of near-surface shearwave velocity by inversion of Rayleigh waves. *Geophysics* 64, 691–700.
- Xia J., Miller, R.D., Park, C.B., Hunter, J.A., Harris, J.B., Ivanov, J., 2002. Comparing shear-wave velocity profiles inverted from multichannel surface wave with borehole measurements. *Soil Dyn. Earthq. Eng.* 22, 181–190.
- Xia J., Miller, R.D., Park, C.B. and Tian, G., 2003. Inversion of high frequency surface waves with fundamental and higher modes. *J. appl. Geophys.*, 52(1), 45–58.
- Xia J., Xu, Y., Chen, C., Kaufmann, R.D. and Luo, Y., 2006. Simple equations guide high-frequency surface-wave investigation techniques, *Soil Dyn. Earthq. Eng.*, 26(5), 395–403.
- Xia J., Miller, R.D., Xu, Y., Luo, Y., Chen, C., Liu, J., Ivanov, J., Zeng, C., 2009. High-frequency Rayleigh-wave method. *J. Earth Sci.* 20, 563–579.
- Xu Y., J. Xia, and R. D. Miller, 2006, Quantitative estimation of minimum offset for multichannel surface-wave survey with actively exciting source: *Journal of Applied Geophysics*, 59, 117–125.

Yılmaz Ö, M. Eser, and M. Berilgen, 2006, A case study of seismic zonation in municipal areas: The Leading Edge, 25, 319–330.